

8-2015

## Quality Assurance Of Advanced Treatment Modalities Using Presage® Dosimeters

Ryan G. Lafratta

Follow this and additional works at: [https://digitalcommons.library.tmc.edu/utgsbs\\_dissertations](https://digitalcommons.library.tmc.edu/utgsbs_dissertations)



Part of the [Medicine and Health Sciences Commons](#), and the [Physics Commons](#)

---

### Recommended Citation

Lafratta, Ryan G., "Quality Assurance Of Advanced Treatment Modalities Using Presage® Dosimeters" (2015). *Dissertations and Theses (Open Access)*. 627.  
[https://digitalcommons.library.tmc.edu/utgsbs\\_dissertations/627](https://digitalcommons.library.tmc.edu/utgsbs_dissertations/627)

This Dissertation (PhD) is brought to you for free and open access by the MD Anderson UTHealth Houston Graduate School at DigitalCommons@TMC. It has been accepted for inclusion in Dissertations and Theses (Open Access) by an authorized administrator of DigitalCommons@TMC. For more information, please contact [digcommons@library.tmc.edu](mailto:digcommons@library.tmc.edu).

**QUALITY ASSURANCE OF ADVANCED TREATMENT MODALITIES USING  
PRESAGE<sup>®</sup> DOSIMETERS**

by

Ryan G. Lafratta, M.S.

APPROVED:

---

Geoffrey Ibbott, Ph.D.  
Advisory Professor

---

David Followill, Ph.D.

---

Narayan Sahoo, Ph.D.

---

James Yang, Ph.D.

---

Susan Tucker, Ph.D.

APPROVED:

---

Dean, The University of Texas  
Graduate School of Biomedical Sciences at Houston

**QUALITY ASSURANCE OF ADVANCED TREATMENT MODALITIES USING  
PRESAGE® DOSIMETERS**

A

DISSERTATION

Presented to the Faculty of  
The University of Texas  
Health Science Center at Houston  
and  
The University of Texas  
MD Anderson Cancer Center  
Graduate School of Biomedical Sciences  
in Partial Fulfillment

of the Requirements

for the Degree of

DOCTOR OF PHILOSOPHY

by

Ryan G. Lafratta, M.S.  
Houston, Texas

August, 2015

**Dedication**

To my dad

For always reminding me

Physics is what physicists do on nights and weekends

To my mom

For always reminding me

There is food in the fridge

To my husband

For always reminding me

He loves me no matter what

## Acknowledgements

I'd like to start by thanking my advisor, Geoffrey S. Ibbott, Ph.D. for his patience, generosity and his time (as precious as it is) over the years. I began my dissertation work knowing nothing about the world of 3D dosimetry and through many confusing analysis sessions, data that defied the laws of physics and optimism that had no basis in reality I have learned more from this project about radiation dosimetry than I ever did in any classroom.

I need to give thanks to my committee who always pushed me to design stronger experiments, use a more critical analysis and for understanding that some months there was simply no new data to present. David Followill and Susan Tucker were members of every committee I ever assembled during my education. Narayan Sahoo and James Yang were close behind. All of my committee members have taken the time to sit with me and go over any question I had. Especially when no one knew the answer and few understood the question.

I'd also like to thank every person that has ever worked for IROC-Houston or the RPC. I have spent almost my entire graduate education surrounded by the most helpful people at MD Anderson Cancer Center. The people at IROC are always willing to help in any way and any student to work there should consider themselves very lucky.

My family is my rock and without them I never would have finished this dissertation. Thank you all so very much for believing in me, comforting me, encouraging me and never once doubting I would finish. My father is an inspiration and I am always grateful to have another physicist to talk through my work, my career path and sometimes to simply discuss anything but work. My mother is a wonder know right when to leave me alone and when to push me further. My husband had no idea what he was getting into marrying a graduate student but never once complained.

Lastly, I once again need to thank Geoffrey Ibbott. You have made me a better scientist. Thanks for never giving up on me.

## Quality Assurance of Advanced Treatment Modalities Using PRESAGE<sup>®</sup> Dosimeters

Ryan G. Lafratta, M.S.

Advisory Professor: Geoffrey Ibbott, Ph.D.

Computer-controlled therapy machines allow for increasingly complex plans, as there are more variables that can be tuned to produce the ideal result. This makes it increasingly difficult to assure the intended calculated dose is being delivered correctly using current techniques that are 2D-based because the resultant dose distributions can differ markedly in various sections of the target. A measurement of composite dose from the entire plan should be included in patient-specific IMRT QA. A volumetric dosimeter such as PRESAGE<sup>®</sup> is able to provide a complete 3D measured dosimetry dataset with one treatment plan delivery. It was hypothesized that a PRESAGE<sup>®</sup> dosimeter would agree with 2D measurements within  $\pm 5\%/3\text{mm}$  using a gamma index analysis. The PRESAGE<sup>®</sup> dosimeter will detect dose discrepancies not detected with 2D measurements resulting in a 5% change in the normal tissue complication probability (NTCP). An optical CT scanner was tested for reproducibility and reliability and a standard operating procedure was created. The PRESAGE<sup>®</sup> dosimeters were extensively tested for dose stability over a range of time for remote dosimetry applications. The effect of temperature changes before, during and after irradiation was investigated. The dosimeter was found to be appropriate for remote dosimetry for relative dose measurements. The IROC-Houston Head and Neck (HN) phantom was imaged with an x-ray CT scanner. One scan used an insert for film and thermoluminescent dosimeter (TLD). A second scan was taken using a PRESAGE<sup>®</sup> insert. An IMRT treatment plan was created and delivered to the phantom using each insert. The gamma index analysis was performed at  $\pm 5\%/3\text{mm}$ . The PRESAGE<sup>®</sup> measurements agreed well with the 2D measurements. Various gamma constraints were applied to the measured data to determine an appropriate passing criterion for 3D gamma analysis. The IMRT treatment plan was modified to induce several different types of treatment and delivery errors. The

plans were analyzed using 2D and 3D gamma analysis. Two plans passed a 2D metric while failing the 3D metric with one of the plans also having a 5% change in NTCP. The hypothesis was proven correct and further work should be considered to bring PRESAGE<sup>®</sup> into a phantom dosimetry program.

## Table of Contents

Signature Page.....	i
Title Page.....	ii
Dedication.....	iii
Acknowledgements.....	iv
Abstract.....	v
Table of Contents.....	vii
List of Illustrations.....	xi
List of Tables.....	xiv
Chapter 1 - Introduction.....	1
1.1    Significance.....	1
1.2    PRESAGE <sup>®</sup> Dosimeters.....	3
1.3    Optical CT.....	5
1.3.1    Principles of Optical CT.....	5
1.3.2    Duke Midsized Optical-CT System for the IROC-Houston (DMOS-IROC) .....	6
1.4    IMRT Quality Assurance and IROC-Houston Phantoms .....	6
1.4.1    Film and TLD Dosimetry.....	7
1.5    Gamma Analysis .....	8
1.6    Normal Tissue Complication Probability (NTCP).....	8
1.7    Hypothesis and Specific Aims .....	9



1.7.1	Specific Aim 1: Determine a standardized protocol for reading dosimeters and performing data analysis .....	10
1.7.2	Specific Aim 2: Assess the capability of PRESAGE <sup>®</sup> dosimeters for remote quality assurance 10	
1.7.3	Specific Aim 3: Examine the use of the system as a clinical quality assurance tool in radiation therapy.....	10
1.7.4	Specific Aim 4: Demonstrate the benefits to the clinic from a measured 3D dataset .	10
Chapter 2 – Specific Aim 1 .....		11
2.1	Rationale .....	11
2.2	Methods.....	13
2.2.1	Light Source Physical Setting .....	13
2.2.2	Camera Field of View .....	14
2.2.3	DMOS-IROC Quality Control .....	15
2.2.4	Projection images .....	17
2.3	Results.....	18
2.3.1	Light Source Physical Setting .....	18
2.3.2	Camera Field of View .....	18
2.3.3	DMOS Quality Control.....	19
2.3.4	Projection images .....	20
2.4	Discussion .....	21
2.4.1	Light Source Physical Setting .....	22
2.4.2	Camera Field of View .....	23

2.4.3	DMOS-IROC Quality Control .....	23
2.4.4	Projection Images.....	23
Chapter 3 - Specific Aim 2.....		25
3.1	Rationale .....	25
3.2	Methods.....	25
3.2.1	Dose Calibrations .....	25
3.2.2	Age and Temperature Dependence .....	30
3.2.3	Readout Procedure .....	34
3.3	Results.....	34
3.3.1	Dose Calibrations.....	34
3.3.2	Age and Temperature Dependence .....	38
3.3.3	Readout Procedure .....	40
3.4	Discussion .....	41
3.4.1	Dose Calibrations.....	41
3.4.2	Age and Temperature Dependence .....	43
3.4.3	Readout Procedure .....	46
Chapter 4 – Specific Aim 3.....		47
4.1	Rationale .....	47
4.2	Methods.....	48
4.2.1	Open field plan.....	48
4.2.2	IMRT Plan.....	54
4.2.3	Gamma Constraints .....	55

4.3	Results .....	56
4.3.1	Open Field Results .....	56
4.3.2	IMRT Plan Results .....	62
4.3.3	Gamma Constraints .....	68
4.4	Discussion .....	70
4.4.1	Open Field Plan .....	70
4.4.2	IMRT Plan .....	71
4.4.3	Gamma Constraints .....	71
Chapter 5 – Specific Aim 4 .....		73
5.1	Rationale .....	73
5.2	Methods .....	74
5.3	Results .....	76
5.4	Discussion .....	79
Chapter 6 – Conclusion .....		83
6.1	Summary .....	83
6.2	Conclusion .....	84
6.3	Future Works .....	85
Appendix .....		86
References .....		97
VITA .....		106

## List of Illustrations

Figure 1-1: bis-(4-dimethylamino-phenyl)-(2-methoxy-phenyl)-methane (o-MeO-LMG) .....	4
Figure 2-1: The DMOS-IROC with the CCD camera on the left and the light source shining from the right. ....	12
Figure 2-2: Example of minimizing edge artifacts by matching the refractive index fluid .....	14
Figure 2-3: Flood Fields over Time .....	16
Figure 2-4: DMOS-IROC Motor .....	16
Figure 2-5: Flow Chart showing the settings for image acquisition and reconstruction.....	17
Figure 2-6: Center of Rotation with incorrect (left) and correct (right) values.....	18
Figure 2-7: Flood Field Center Value over time .....	20
Figure 2-8: Images Averaged line profiles.....	21
Figure 3-1: The film phantom for dose calibrations was created from a used PRESAGE <sup>®</sup> dosimeter. Film was sandwiched between the two levels and compared to a dosimeter from the batch of PRESAGE <sup>®</sup> being calibrated. ....	26
Figure 3-2: An example of a film irradiated with overlapping dose areas which created 4 dose levels for the calibration curve. ....	27
Figure 3-3: The high-impact phantom containing a cuvette cutout (left) with cuvettes inserted. A close up of the cuvettes is shown on the right.....	29
Figure 3-4: Set up for storage and temperature irradiations.....	32
Figure 3-5: Dosimeters being brought to extreme cold or hot for irradiation. The equilibration was done in a water bath for irradiation. ....	33
Figure 3-6: Film Calibration for film used in PRESAGE <sup>®</sup> calibration phantom and HN phantom irradiations. Error bars indicate one standard deviation.....	35
Figure 3-7: PRESAGE <sup>®</sup> Batch 01-13 Dose Response .....	36
Figure 3-8: 12 Dose Response of Cuvettes Containing PRESAGE <sup>®</sup> .....	36

Figure 3-9: Dose Response of Cuvettes Containing PRESAGE® Batch 01-13 .....	37
Figure 3-10: Batch 01-13 Dose Response Comparison .....	38
Figure 3-11: Storage Temperatures with repeated post scans over time.....	38
Figure 3-12: Temperature changes prior to and post irradiation.....	39
Figure 3-13: Temperature changes at irradiation .....	39
Figure 3-14: Initial Readout with Varying Irradiation Temperature.....	40
Figure 4-1: The HN phantom and imaging insert (left). A CT slice of the imaging insert with labeled structures (right).....	48
Figure 4-2: film/TLD Insert with structures and TLD contoured .....	49
Figure 4-3: PRESAGE® Insert with the dosimeter surface contoured (orange) and a second contour drawn 5 mm inside the surface of the dosimeter (green) .....	50
Figure 4-4: Phantom setup with laser alignment to BBs.....	51
Figure 4-5: Film Profile locations .....	53
Figure 4-6: Right-Left film profile from Trial 1 of APRL plan.....	57
Figure 4-7: Superior-Inferior film profile from Trial 1 of APRL plan .....	57
Figure 4-8: Anterior-Posterior film profile from Trial 1 of APRL plan .....	58
Figure 4-9: 2D Gamma results for film at 5%/3mm in the axial (left) and sagittal (right) planes for Trial 1 of APRL Plan .....	58
Figure 4-10: Dose Response for APRL PRESAGE® Batch.....	59
Figure 4-11: PRESAGE® Right-Left dose profiles for APRL plan .....	60
Figure 4-12: PRESAGE® Superior Inferior Profiles for APRL plan .....	60
Figure 4-13: PRESAGE® Anterior-Posterior profiles for APRL plans .....	61
Figure 4-14: Right-Left Film Profiles for Trial 1 of IMRT plan.....	62
Figure 4-15: Superior-Inferior film profile for Trial 1 of IMRT plan.....	63
Figure 4-16: Anterior-Posterior film profile for Trial 1 of IMRT plan.....	63

Figure 4-17: 2D Gamma results for film at 5%/3mm in the axial (left) and sagittal (right) planes for Trial 1 of IMRT plan.....	64
Figure 4-18: Dose Response Curve for IMRT PRESAGE <sup>®</sup> Batch .....	65
Figure 4-19: Right-Left PRESAGE <sup>®</sup> profiles for IMRT plan.....	66
Figure 4-20: Superior-Inferior PRESAGE <sup>®</sup> profiles for IMRT plan.....	66
Figure 4-21: Anterior-Posterior PRESAGE <sup>®</sup> profiles for IMRT plan .....	67
Figure 4-22: IMRT Trial 1 Gamma Index at 5%/3mm with 96% of pixels passing.....	68
Figure 5-1: NTCP modeling from CERR for Trial 3 dose measurement .....	76
Figure 5-2: Dose Volume Histogram for the Extended Parotid plan and Trial 3 measurement .....	80

## List of Tables

Table 2-1: Center of Rotation Settings.....	19
Table 2-2: Example of monthly checklist posted in scanning workroom to be initialed by user performing QC .....	20
Table 3-1: MU delivered to each film square .....	28
Table 3-2: MU delivered to 12 cuvette study.....	30
Table 4-1: DMOS Settings for HN Phantom Irradiations.....	53
Table 4-2: CERR coordinates for 2D Gamma Comparison.....	54
Table 4-3: IMRT Dose Prescription.....	54
Table 4-4: Average TLD Results from 3 APRL Irradiations.....	56
Table 4-5: PRESAGE <sup>®</sup> average gamma results at 5%/3mm for APRL plans .....	61
Table 4-6: Average TLD Results for IMRT Plan .....	62
Table 4-7: PRESAGE <sup>®</sup> average gamma results at 5%/3mm for the IMRT plan .....	67
Table 4-8: Pass rates for 3 levels of gamma constraints .....	69
Table 5-1: NTCP values from Measured Dose .....	76
Table 5-2: 2D and 3D Gamma Results at 5%/3mm.....	78
Table 5-3: Gamma Index and NTCP results. Highlighted results passed a 2D evaluation and failed a 3D evaluation. ....	78
Table 7-1: TLD Results for Trial 1 from APRL Plan .....	86
Table 7-2: TLD Results for Trial 2 from APRL Plan .....	86
Table 7-3: TLD Results for Trial 2 from APRL Plan .....	87
Table 7-4: 2D Gamma Results at 5%/3mm for Trial 1 from APRL Plan.....	87
Table 7-5: 2D Gamma Results at 5%/3mm for Trial 2 from APRL Plan.....	87
Table 7-6: 2D Gamma Results at 5%/3mm for Trial 3 from APRL Plan.....	88
Table 7-7: TLD Results for Trial 1 from IMRT Plan .....	88

Table 7-8: TLD Results for Trial 2 from IMRT Plan ..... 88

Table 7-9: TLD Results for Trial 3 from IMRT Plan ..... 89

Table 7-10: Percentage of passing pixels for various Gamma Index Restraints for Trial 1 from IMRT  
Plan..... 90

Table 7-11: Percentage of passing pixels for various Gamma Index Restraints for Trial 2 from IMRT  
Plan..... 91

Table 7-12: Percentage of passing pixels for various Gamma Index Restraints for Trial 3 from IMRT  
Plan..... 92



## Chapter 1 - Introduction

### 1.1 Significance

Modern therapy machines are mechanically precise and computer-controlled, allowing for dynamic deliveries that can include varying dose rates, beam apertures, collimator orientations, gantry angles and couch positions in a continuous fashion. A treatment plan that utilizes these tools is volumetric in design and usually has significant dose gradients. Dose verification of these complex treatments is becoming increasingly important in the clinic as computer errors in delivery can occur and treatment planning systems (TPS) might not be fully commissioned to accurately calculate every possible variable available in delivery. Since these dose distributions normally are designed to conform to irregularly shaped targets, traditional dosimetry methods including ion chamber and planar film measurements become increasingly time consuming and may not be sufficiently comprehensive to verify correct delivery (1). The dose distributions for Intensity Modulated Radiation Therapy (IMRT) require quality assurance (QA) checks of the cumulative dose delivered and not just the an individual segment of delivery (2). Many QA programs for IMRT focus on ion chamber measurements with planar dosimetry. The gamma function (3) is widely used to compare a measured planar dose distribution to the distribution calculated by the TPS. Studies have shown this method of single planar dosimetry can produce gamma analysis results that are insensitive to the changes in measured and calculated IMRT dose distributions (4, 5). These studies suggest that a measurement of composite dose from the entire plan be included in patient-specific IMRT QA. A volumetric dosimeter such as PRESAGE<sup>®</sup> is able to provide a complete 3D measured dosimetry dataset with one treatment plan delivery.

The Imaging and Radiation Oncology Core Houston Quality Assurance Center (IROC-Houston) uses anthropomorphic phantoms as an end-to-end test for quality assurance at institutions participating in clinical trials. The phantoms are able to test imaging, treatment planning, patient

setup and treatment delivery. At this time, the phantoms use thermoluminescent dosimeters (TLD) and radiochromic film to measure dose and dose distributions, respectively. This design yields only two or three planes of dose information, depending on the phantom, to compare to the treatment plan calculated data. From data compiled in 2008, almost 30% of institutions failed to deliver dose distributions, using the IMRT Head and Neck (HN) phantom, that agreed with their treatment plans within the constraints of 7%/4 mm (6). Having a full 3D dose distribution could help decipher the type of error (positioning, MLC malfunction etc.) that could have occurred during the process and help IROC-Houston with appropriate QA recommendations for the institution.

The overall clinical value of 3D dosimetry has not been widely tested. Difficulty in maintaining consistent formulations for these dosimeters, complicated equipment for fabrication, expensive and time-consuming readout systems, and the learning curve for the person conducting the measurements have factored into the slow uptake in the clinic. While several groups have been able to use 3D dosimeters for clinical purposes there have been no investigations into the ability of volumetric data to significantly impact clinical practices (7-9). For example, it is not known whether easily attainable volumetric data could affect clinical practices for patient quality assurance. Are we able to estimate changes in patient outcome based on the difference in the calculated and delivered dose distribution? Would the plan then be considered clinically unacceptable after measured QA and re-planned? A criterion would have to be established to designate a threshold at which treatment would be postponed due to volumetric data results for further inquiry.

Another use would be the remote dosimetry aspect for 3D phantoms. As mentioned earlier, almost 30% of institutions from 2008 and before did not pass the credentialing test with the head and neck IMRT phantom. A volumetric dataset might capture even more errors, might be able to determine the source of the error, or might capture a lower percentage of data points exceeding a 2-D QA Pass Criteria that would allow False Positive in QA.

With routine radiation therapy treatments becoming more advanced, QA protocols need to keep pace for physicists to ensure the safe and reliable delivery of the intended treatment. 3D dosimeters have matured to the point that common clinical use could be feasible. Research into situations where a measured 3D dataset would be of greater value than the current process of 2D dosimetry is necessary.

## 1.2 PRESAGE<sup>®</sup> Dosimeters

In 1950, Day and Stein (10) introduced the idea to use radiosensitive gels to measure radiation. The modern use of gels for radiation dosimetry resulted from work done by Gore in 1984 (11). Since then, work has focused on two types of gel dosimeters, containing either ferrous sulphate or a polymer.

Most work initially involved the use of Fricke dosimeters ( $\text{Fe}(\text{SO}_4)$ ) blended in water-equivalent gels. Gore *et al* demonstrated that magnetic resonance images (MRI) indicate the concentration of  $\text{Fe}^{3+}$  produced, which is related directly to absorbed radiation dose (11). Gore's work to combine a chemical dosimeter, gelling agent, and imaging readout yielded the first truly 3D dosimeter for radiotherapy. However, the general use of the initial dosimeter was hindered by difficulties in making the gel dosimeter and the rapid diffusion of the ions in the medium. Variations of composition were tested but diffusion remained a problem for this type of gel dosimeter(12). In addition, access to an MRI machine in most hospitals is limited and expensive. Optical computed tomography (OCT) systems were tested as an alternative readout method but the results were not compelling as compared to MRI since these dosimeters lessened light attenuation mainly by scattering and not absorption.

The next generation of gel dosimeters involved the use of polymers (notably polyacrylamide) rather than ferrous sulfate. These dosimeters were also read out using MRI. However, these dosimeters were sensitive to oxygen because it scavenges free radical initiators of

the polymerization reaction. Many variations of polymer gel dosimeters were investigated (12-14) but this type of gel dosimeter has experienced only limited clinical acceptance because of the complex manufacturing process required to eliminate oxygen from the gel system as well as the difficulty in containing the gels in some sort of anthropomorphic phantom or shape. Again, the need for MRI readout was a hindrance and OCT readout suffered from the same inadequacies as for the Ferrous Sulfate gels.

In 2003, a new dosimeter named PRESAGE<sup>®</sup> [Heuris Pharma, LLC, Skillman, NJ] was introduced (15) and was more fully characterized in 2006 (16). This dosimeter is a solid polyurethane dosimeter with a leuco-dye, o-MeO-LMG, synthesized by Heuris Pharma. Free radical initiators change the leuco malachite green to malachite green causing a change in color and therefore optical density after exposure to ionizing radiation. Quantifying the change in optical density leads to the determination of radiation dose distribution.

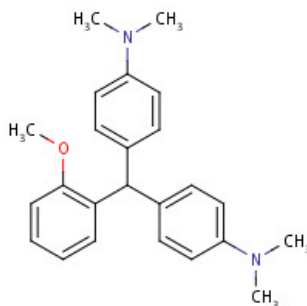


**Figure 1-1: bis-(4-dimethylamino-phenyl)-(2-methoxy-phenyl)-methane (o-MeO-LMG)**

This dosimeter has several advantages over gel dosimetry including its insensitivity to oxygen contamination, stable optical absorption for wide dose range and a solid state that can be machined to any shape and does not require an outer container (16). Certain gels can often have a diffusion problem that is not seen in PRESAGE<sup>®</sup> (17). PRESAGE<sup>®</sup> is light absorbing rather than light

scattering allowing it to be read using an optical CT technique (16). Studies have been conducted to show at ~633 nm (the red wavelength) there is a maximum change in the radiation induced optical density (18).

Several studies have been performed investigating the use of PRESAGE®. The linearity of the dose response at low energies has been confirmed by several sources (16, 19). A post-irradiation stability using has been marked at 5 days by Guo *et al.* (18). Skyt *et al.* determined that temperature effects on PRESAGE® has an effect on dose response (20). These studies were all conducted with cuvettes with large volume measurements were either assumed to hold true or are pending future research.

An optical CT of the PRESAGE® dosimeter is performed to capture the volumetric dataset. The principles are described in the next section.

### 1.3 Optical CT

#### 1.3.1 Principles of Optical CT

Beer's Law describes how light and X-rays are attenuated through a medium. By using the linear attenuation coefficient,  $\mu$ , of the medium the intensity of light measured at distance  $s$  along the ray path is given by

$$I = I_0 \exp \left[ - \int_{ray\ path} \mu(s) ds \right] \quad \text{Equation 1-1}$$

where  $I_0$  is the light intensity without the sample in the path of the light. Obtaining the projections at different rotation angles creates a sinogram in Radon space. The optical attenuation of the sample can then be found using filtered back-projection as in x-ray CT (21). Note that the intensity  $I$  is related to optical density as  $OD = -\log_{10}(I/I_0)/\text{sample length}$ . Typically, the optical density of a dosimeter such as film is taken as a whole and the OD is dimensionless. However, with 3D

dosimeters OD has units of  $\text{cm}^{-1}$  as OD is an intensive property of the sample that is imaged within each voxel.

In broad beam optical CT, such as we use with PRESAGE<sup>®</sup>, a uniform light source is measured with a charge-coupled device (CCD) camera. At each projection angle on a PRESAGE<sup>®</sup> phantom, the Radon Transform (RT) is used to create a 2D plane of data providing a row of the sinogram in RT space for every slice of the dosimeter at one time. Summing projections at multiple angles creates a full sinogram that can be deconvolved into a true 3D reconstruction.

### ***1.3.2 Duke Midsized Optical-CT System for the IROC-Houston (DMOS-IROC)***

Rather than a Point Source of light, for PRESAGE<sup>®</sup> readout we use a broad beam optical CT system designed by Duke University (22). It consists of a fixed, uniform line light source measured by a charge-coupled device (CCD) camera. The dosimeter is placed in a water bath on a rotating pedestal and the captured data at each angle is combined to create the 3D data set.

The system came with operating instructions addressing how to image and reconstruct a dosimeter but the procedures did not detail which settings to input therefore it was necessary to create a set of uniform procedures for collecting raw data and its subsequent analysis for our purposes. Image capture is run in LabVIEW [National Instruments, Austin, TX] while reconstruction is completed with MATLAB<sup>®</sup> [MathWorks, Natick, MA]. The final reconstruction is saved in a file intended for use with CERR (The Computational Environment for Radiotherapy Research), a MATLAB-based program that can compare dose distributions created in many planning systems.

## **1.4 IMRT Quality Assurance and IROC-Houston Phantoms**

The dose distributions for Intensity Modulated Radiation Therapy (IMRT) require quality assurance checks of the cumulative dose delivered and not just the an individual segment of delivery (2). Many QA programs for IMRT focus on ion chamber measurements with planar dosimetry. The gamma function (3) is widely used to compare a measured planar dose distribution to the distribution to the distribution calculated by the TPS. Studies have shown this method of single planar dosimetry

can produce gamma analysis results that are insensitive to the changes in measured and calculated IMRT dose distributions (4, 5). These studies suggest that a measurement of composite dose from the entire plan be included in patient-specific IMRT QA. A composite plan is tested by IROC-Houston and will be used in this study.

#### ***1.4.1 Film and TLD Dosimetry***

The phantom used in this project uses film and TLD to measure dose. The phantom is fitted for double-loaded capsules of LiF TLD 100 powder. In thermoluminescent (TL) detectors, incident radiation releases electrons from the valence band to the conduction band and the electrons are then captured by various trapping centers (23). When exposed to heat, these trapped electrons are then able to return to the conduction band while releasing light. A photomultiplier tube (PMT) records the amount of light and a glow curve is produced comparing the light signal to the temperature at the time of emission. The area under the glow curve corresponds to the number of photons released. Using this signal (T), along with correction factors for energy ( $K_e$ ), linearity ( $K_l$ ), fading ( $K_f$ ) and system sensitivity (S) the dose can be calculated using Equation 1-2.

$$D = T \times K_e \times K_l \times K_f \times S \quad \text{Equation 1-2}$$

EBT2 Gafchromic film (ISP, Wayne, NJ) is a self-developing yellow film commonly used in IMRT QA comprised of an active layer laminated by two polyester layers with an absorbance spectrum near 636 nm (24). The dose has been found to stabilize by 24 hours post-irradiation and can be digitized with both flatbed scanners and film densitometers.

## 1.5 Gamma Analysis

There are many ways to compare two dose distributions. A dose difference test compares the dose difference in distributions point by point is overly sensitive in a steep dose gradient since small offsets in dose distribution are shown as large dose difference in the steep dose gradients (3). The distance to agreement test was developed to overcome this sensitivity by independently searching each point of one dose distribution to locate the nearest identical dose value in the second dose distribution (25). This test had the opposite sensitivity issues by magnifying differences in the shallow dose gradient. Low *et al.* developed the gamma analysis tool combining dose and spatial information in a single test to offset the sensitivities of using the tests separately (26). The dose distributions are re-normalized in a space with dose and spatial coordinates where the axis are the acceptance criteria and the center is the reference point from one dose distribution. The minimum distance from the reference point to the measured point of the second distribution is the gamma index.

Literature has shown volumetric datasets could increase the passing rate of a gamma analysis while others have found the opposite result when comparing different dosimeter types as was done in this study (27, 28).

## 1.6 Normal Tissue Complication Probability (NTCP)

Treatment plans are assessed by their ability to control the tumor while sparing normal tissue in surrounding sites. The NTCP is a model that helps estimate the risk of complication to an organ or tissue based on the dose delivered to a volume. The most widely used NTCP model is the Lyman-Kutcher-Burman (LKB) model (29). This model combines the Lyman NTCP model (30) with the Kutcher and Burman DVH modification for partial organ irradiation (31).



$$NTCP(D, v) = \frac{1}{\sqrt{2\pi}} \int_{-\infty}^t e^{-t^2/2} dt \quad \text{Equation 1-3}$$

where

$$t = \frac{D - D_{50}(v)}{m \cdot D_{50}(v)} \quad \text{Equation 1-4}$$

Equations 1-2 and 1-3 describe the LKB model that is a function of dose ( $D$ ) and volume ( $v$ ).  $D_{50}(v)$  is the 50% tolerance dose for uniform partial-organ irradiation to the volume  $v$  (32) and is described by equation 1-4. The variables  $m$  and  $a$  are found by fitting tolerance doses:  $m$  characterizes the slope of the dose response-function and  $a$  characterizes the volume effect.

$$D_{50}(v) = D_{50}(1) \cdot v^{-1/a} \quad \text{Equation 1-5}$$

$$EUD = \left( \sum_i v_i D_i^a \right)^{1/a} \quad \text{Equation 1-6}$$

The equivalent uniform dose (EUD) shown in equation 1-5 was introduced by Niemierko (33) and is used by CERR to evaluate the NTCP by replacing the total dose  $D$  in equation 1-4 with  $EUD$  (34). By registering the PRESAGE<sup>®</sup> dose distribution to the treatment plan using CERR, the NTCP can be calculated for both measured and calculated dose distributions using the plan's organ contours to obtain volume (28). This allows for a quantifiable metric for change in tumor control should the dose distributions differ.

## 1.7 Hypothesis and Specific Aims

The hypothesis for this project is that dose distributions for complex dose distributions measured with the PRESAGE<sup>®</sup> 3D dosimeter will agree with 2D measurements to within  $\pm 5\%/3\text{mm}$  using a gamma index analysis. The PRESAGE<sup>®</sup> dosimeter will detect dose distribution discrepancies for complex treatments not detected by 2D planar measurements that will result in a 5% difference in NTCP. This was tested with four specific aims.

***1.7.1 Specific Aim 1: Determine a standardized protocol for reading dosimeters and performing data analysis***

This aim verifies the alignment of the optical CT scanner used to image the dosimeters and creates a quality assurance protocol to verify the uniformity and constancy of optical density prior to data acquisition. A standard operating procedure was created to ensure optical scanning would be reproducible independent of the user.

***1.7.2 Specific Aim 2: Assess the capability of PRESAGE® dosimeters for remote quality assurance***

A “standard” calibration scheme was developed. Age dependence of the dosimeter was assessed and the influence (if any) of the readout procedure on the dosimeter was quantified. Effects of shipping to offsite facilities were evaluated to determine if phantom studies could be conducted remotely.

***1.7.3 Specific Aim 3: Examine the use of the system as a clinical quality assurance tool in radiation therapy***

Treatment plans were created starting with open fields and moving towards complex, clinically relevant plans. Data from irradiated dosimeters was compared against a standard 2D measurement quality assurance test and the computed plan from the treatment planning system (TPS). Gamma index analyses at different constraints were applied for comparison.

***1.7.4 Specific Aim 4: Demonstrate the benefits to the clinic from a measured 3D dataset***

Using NTCP models, the complication probability was calculated from the 3D dose distributions from the TPS calculation and from the PRESAGE® measurements.

## Chapter 2 – Specific Aim 1

### 2.1 Rationale

The first specific aim is to determine a standardized protocol for reading dosimeters and performing data analysis. This aim is intended to prepare and optimize the Duke Midsized Optical CT Scanner for the IROC-Houston (DMOS-IROC) [Duke University, Durham, NC] for use as a routine quality assurance tool in the remote phantom program.

Duke University has been working on optical CT scanners for 3D dosimetry and PRESAGE<sup>®</sup> for several years (35, 36). The DMOS-IROC was built at Duke University specifically for the IROC-Houston's use. The scanner uses a 633 nm light source since this is the optical absorption wavelength for PRESAGE<sup>®</sup>. A photograph of the scanner is shown in Figure 2-1. The light source passes through a diffuser (to create a uniform field) and a band pass filter leaving the first of a matched set of telecentric lenses before entering a tank filled with a mixture of octyl salicylate, octyl cinnamate and mineral oil to match the refractive index of the dosimeter and minimize the refraction and reflection of incident light on the dosimeter. The dosimeter sits on a rotating stage and as the dosimeter rotates the light then enters the second telecentric lens and is captured by a CCD camera.



**Figure 2-1: The DMOS-IROC with the CCD camera on the left and the light source shining from the right.**

Initial commissioning tests were performed at Duke University before installation at IROC-Houston (37) and these commissioning tests were repeated for verification in a separate study.

No quality assurance protocol was suggested for the scanner at installation so one needed to be developed to confirm whether any measured dose difference was due to irradiation and not improper imaging. Discrepancies in dose distributions can be difficult to discern in anthropomorphic phantoms and variables should be contained when possible. Procedures for QA on the scanner and standardization of use across several users need to be established prior to performing patient QA.

The first specific aim was separated into four separate sections:

- Setting the physical light source
- Setting the camera's field of view and the center of rotation for reconstruction
- Creating a quality control program
- Finding the optimal number of averaged images for each projection angle

## 2.2 Methods

### 2.2.1 Light Source Physical Setting

One of the most important settings for the DMOS-IROC is the light source. The main objective is to set the LED light source to create a uniform flood field with as much light as possible passing through the system. Equation 2-1 describes how the dose is measured where  $I_{pre}$  is the un-irradiated pre-scan camera reading in the center of the dosimeter,  $I_{irradiated}$  is the desired minimum camera reading,  $s$  is the sensitivity ( $\Delta OD/Gy/cm$ ) and  $x$  is the irradiated path length through the dosimeter. The change in OD is  $\log(I_{pre}/I_{irradiated})/x$ . As previously stated in Section 1.3.1, with 3D dosimeters OD has units of  $cm^{-1}$  or  $mm^{-1}$  as OD is an intensive property of the sample that is imaged within each voxel. The amount of light through the system partly determines the dynamic range that can be achieved. The amount of light that exits the dosimeter decreases as the light input from the source decreases. When too little light is transmitted to the camera the dose that can be delivered to the dosimeter is limited.

$$Dose = \frac{\log\left(\frac{I_{pre}}{I_{irradiated}}\right)}{s \cdot x} \quad \text{Equation 2-1}$$

An uneven flood field limits the usable Field of View (FOV) for dosimeters. With varying phantom sizes in the IROC-Houston phantom program, a maximized uniform flood field is necessary.

To find an optimal setting, the light source was moved towards and away from the lens as well as rotated. Band pass filters and diffusers were interchanged until the most uniform field could be created. The light source was then affixed to the system and not changed.

### 2.2.2 Camera Field of View

The camera FOV can be sized to only show the dosimeter rather than capturing an image of the majority of the tank. The area of the FOV corresponds to the image size that must be stored and the time needed for reconstruction. Using the smallest FOV possible saves valuable disk space and shortens the reconstruction. As the FOV changed, the center of rotation for the filtered back projection also changed. The center of rotation for each FOV needed to be defined for proper reconstruction.

To image a dosimeter first the dosimeter is placed in the tank. The fluid is matched to the dosimeter by changing the concentration levels of the fluid until optical edge artifacts are removed as shown in Figure 2-2.

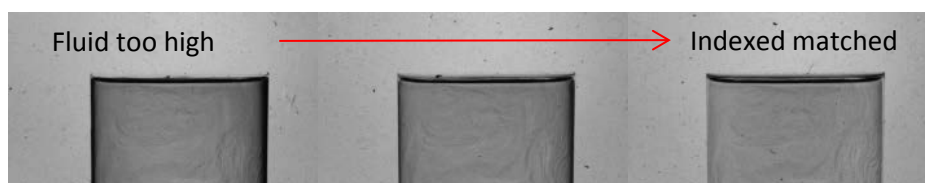


**Figure 2-2: Example of minimizing edge artifacts by matching the refractive index fluid**

The captured image data is run in LabVIEW and reconstruction is completed with MATLAB<sup>®</sup>. The rotation angle and number of projections is input into the acquisition software. The flood image was acquired without the dosimeter in the aquarium and was be a single projection with 200 images averaged. The dark image was taken in the same manner but with the light physically blocked from reaching the camera. The flood and dark images were taken for each dosimeter. The sinogram was created using the flood and dark field corrected projection images. The pre-irradiation sinogram and post-irradiation sinogram were subtracted to produce a sinogram that was comprised entirely of change in optical density. At this point, the reconstruction width of each voxel was selected. The subtracted sinogram was created and then reconstructed into a 3D cube of data by filtered back projection with a user defined filter and center of rotation. This cube was exported into

the CERR environment for further evaluation that could include CT-dose profiles and dose calculations in the area of interest.

A FOV was chosen for each size dosimeter. A cylindrical dosimeter that fits in the FOV was irradiated with a single 4 cm by 4 cm dose field that fits completely within the dosimeter. During reconstruction, the user was asked to select the center of rotation. The center was moved until the reconstruction was done correctly and was recorded. This was qualitatively decided when the outer edge of the dosimeter is a single circle and the edge of the square field is sharp. The center of rotation was found for different size FOVs for consistency and reproducibility as new sizes of dosimeters are ordered. A list of commonly ordered dosimeter sizes was created along with the appropriate center of rotation. While this experiment focused on the dosimeters used for this project, the list was continually updated as different dosimeters were created for other experiments using the DMOS-IROC. A spreadsheet with the center of rotations was saved to the Desktop of the DMOS-IROC computer for easy access for all users of the system.

### ***2.2.3 DMOS-IROC Quality Control***

To use 3D dosimetry as a part of an official remote dosimetry service, quality control on the IROC-Houston side also needs to be implemented. Monthly quality assurance should be done to verify the stability of the light source and camera as a system.

Three separate checks of the system's function are tested at least on a monthly schedule. First, the flood field is checked to ensure the raw counts without a dosimeter are still hovering near 3500 raw counts with the camera shutter set at 150 to compare to installation flood field. As major changes occur, the "baseline" flood can be reassigned. Major changes include realignment, new lenses, new diffusers and color changes in the fluid. Figure 2-3 shows examples of changing "baseline" flood fields over scanner upgrades (top row) and an example of subsequent flood fields captured for monthly stability check (bottom row)

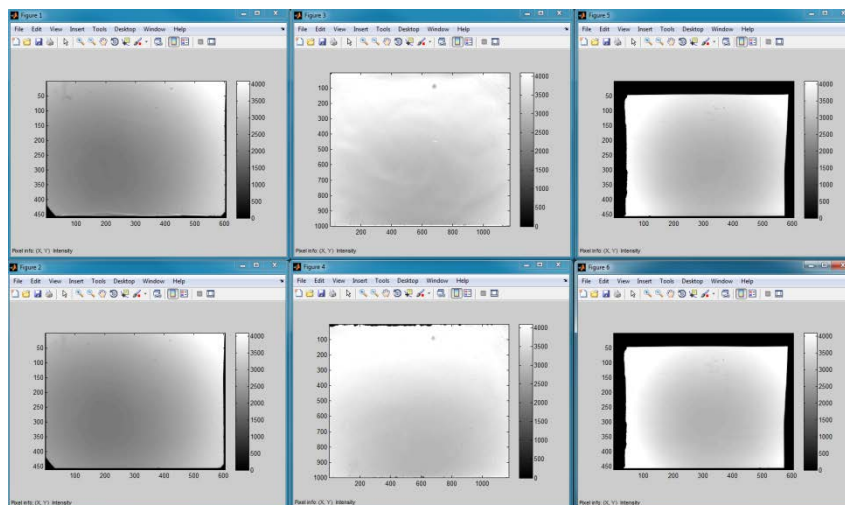


**Figure 2-3: Flood Fields over Time**

The second check of the system is the motor start position and the physical step size compared to the software's command. The start position of the motor can be reset accidentally if the applications are not closed properly at the end of a scan or if aborted incorrectly in the middle of a scan. Checking the start position ensures the pre and post scans are aligned correctly. Physical hash marks on the motor were checked for alignment when the motor was sent to 0 degrees. The motor (Figure 2-4) was then told to move 5 and 10 degrees and the hash marks were recorded.

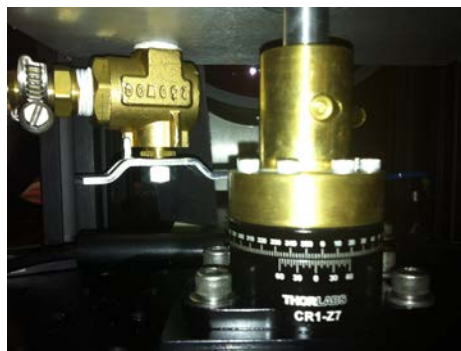


**Figure 2-4: DMOS-IROC Motor**

The third check of the system is the tank check. Seals are checked for fluid leakage around the glass and at the base. Filter tubes are checked for cracking and aging.



### 2.2.4 Projection images

The use of the DMOS-IROC was outlined in Section 2.2.2. A flowchart shown in Figure 2-5 describes the user inputs for image acquisition (DMOS-IROC settings) and reconstruction.

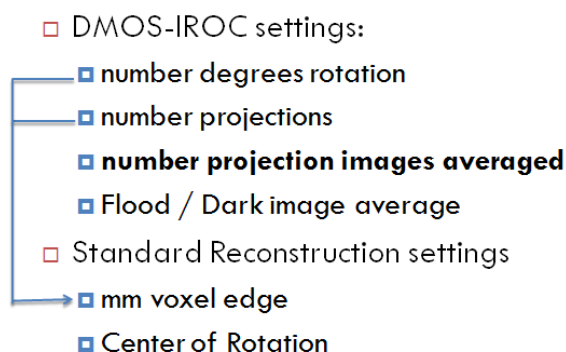


**Figure 2-5: Flow Chart showing the settings for image acquisition and reconstruction**

The number of degrees per rotation and the number of projection images determined the minimum voxel edge length for the reconstructed image. The flood and dark image average number of images is set to 200 for all irradiations. This was the maximum number of images that could be captured. The center of rotation for the reconstruction was determined using the methodology described in Section 2.2.2. The final user input determined was the number of projection images averaged together for each degree of rotation. This was the time limiting portion of scanning.

A dosimeter was placed in the tank and images averaged input was set to the default setting of 25. This setting takes 25 projection images and averages them together as one projection. The signal to noise ratio increases with increasing projections to average. The scan time also increases with increasing images averaged. This number was lowered in increments of 5 until 10 images had been reached. Then the number of averages was decreased in increments of 1 until 7 images had been reached. The original reconstruction (with 25 images averaged) was used as a baseline until a noticeable difference was recorded. The minimum projection average was used for all other image acquisitions.

## 2.3 Results

### 2.3.1 Light Source Physical Setting

The lens was set to allow as uniform a flood field as possible. The DMOS-IROC has brighter outer edges as compared to the center. With the maximum field of view, the center flood image had a raw count of 3500. Using the FOV for the HN phantom the flooded out region (=4500) was minimized to the outer corners and outside the field of the dosimeter.

### 2.3.2 Camera Field of View

Figure 2-6 shows an example of changing the center of rotation value. On the left is an incorrect value of 295 while on the right is a correct value of 316.

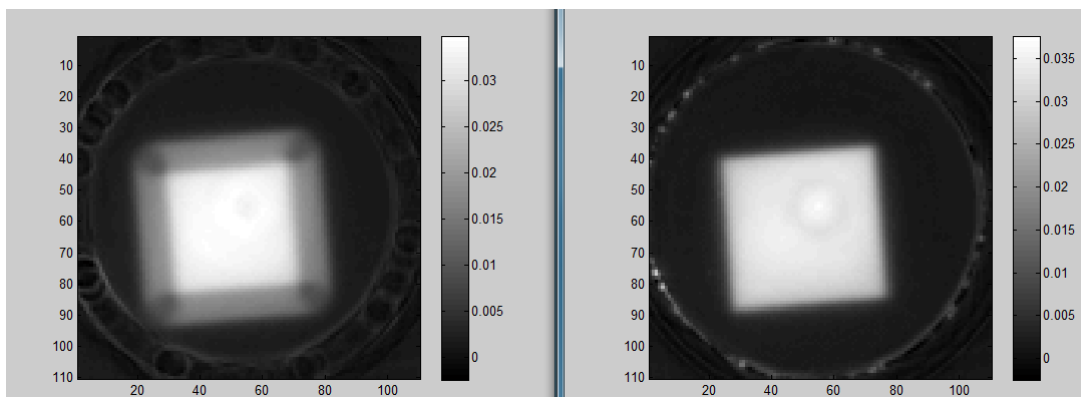


**Figure 2-6: Center of Rotation with incorrect (left) and correct (right) values**

Table 2-1 lists the camera FOV options and matching center of rotation (COR) values.

Dosimeter	Left	Top	Width	Height	COR
<b>Small Standard (Prior to 12/2011)</b>	120	150	600	454	291
Large Standard (Prior to 12/2011)	<b>100</b>	<b>110</b>	<b>605</b>	<b>461</b>	<b>316</b>
1 kg HN Insert	<b>160</b>	<b>30</b>	<b>1170</b>	<b>1000</b>	<b>585</b>
<b>Spine Insert</b>	250	40	1000	960	520
<b>7cm x 9cm Nominal Dosimeter</b>	250	280	1000	760	515
<b>Cyberknife Standard</b>	320	194	800	846	430
<b>Breast Phantom</b>	89	0	1303	1040	660

**Table 2-1: Center of Rotation Settings**

The two bolded values were used in this study. Note the change after December 2011 when the system's camera was upgraded and therefore new values had to be quantified. Other dosimeters used in separate experiments are also listed demonstrating the range of customization for the DMOS-IROC.

### **2.3.3 DMOS Quality Control**

A chart of the flood field over the course of experiments in this project is shown in Figure 2-7. Gaps in information are due to the system being down for maintenance, upgrades or not in use at that time. The dark field has not changed in any measurable way. After August of 2013, the 3D dose lab group began varying formulations of PRESAGE<sup>®</sup>, all with separate refractive indexes. From this point on the flood field could change on a scan by scan basis and monthly flood field checks were discontinued.

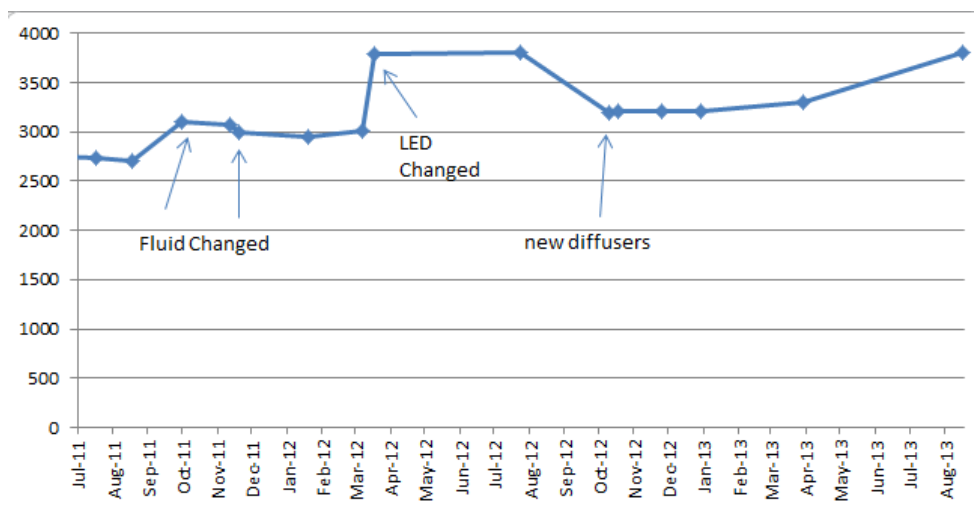


**Figure 2-7: Flood Field Center Value over time**

The motor was out of its start position 8 times since February 2011 when it was added to the QA check. All 7 were accounted for as times when LabView either crashed mid-scan or was shut down improperly. LabView crashes when settings are selected out of order but users have been trained to reset the motor after a crash and to verify the motor's start position prior to any scanning.

Hose Integrity	Leaks	Motor Position	Flood Field	Lens Offset	Date / initials
<b>Month</b>					

**Table 2-2: Example of monthly checklist posted in scanning workroom to be initialed by user performing QC**

A checklist (Table 2-2) was posted in the scanning workroom to perform daily checks and to sign off on monthly checks. Monthly, the seals are checked for leaking fluid, the filter tubes are checked for leakage near the tank and filter and for physical degradation by the filter pump. The tubing is exchanged every 6 months due to the physical wear from the systolic filter pump. The motor start position is verified and the lenses are physically checked for any offset.

### 2.3.4 Projection images

To prevent excessive downsampling of the image during reconstruction an adequate number of projections needed to be acquired to satisfy the Nyquist sampling criteria. For control dosimeters

and IMRT this was defined at 1 degree per rotation and 360 projections allowing for multiple reconstruction sizes to be available post-irradiation.

Figure 2-8 shows a line profile through the same dosimeter as various number of average images was acquired.

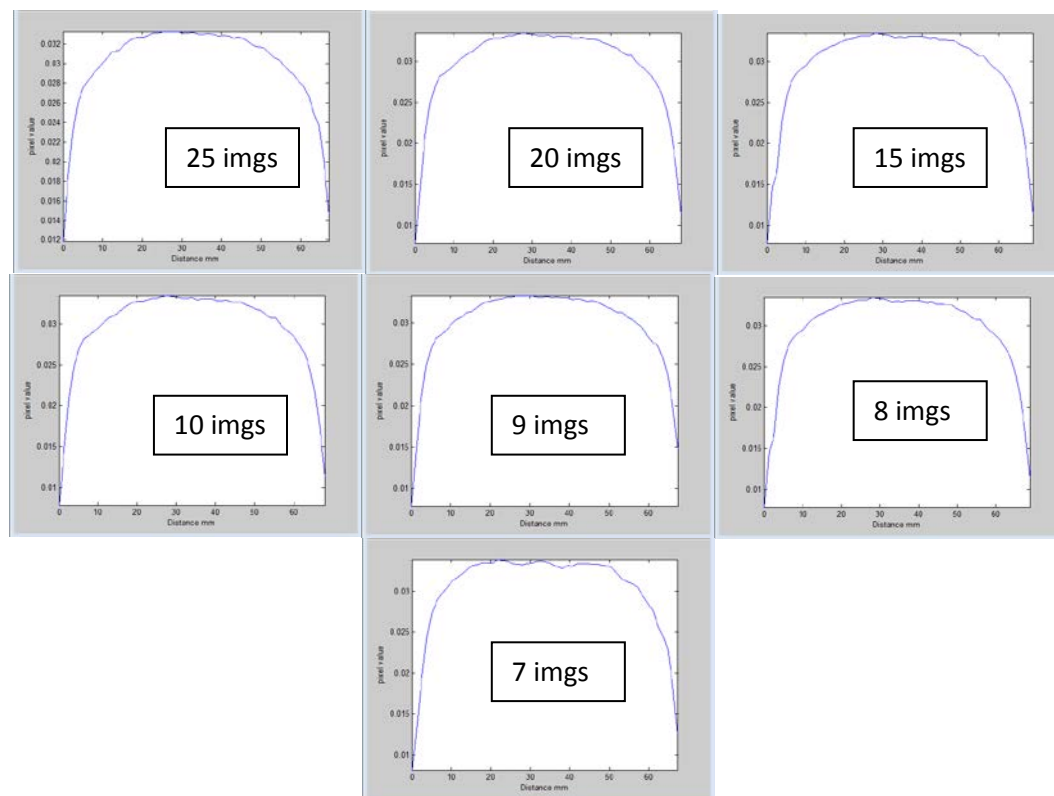


**Figure 2-8: Images Averaged line profiles**

The projection image data was compared from 25 images to 7. A significant difference was not recorded until 7 images were averaged. Eight images averaged per projection was recommended for standard scans.

## 2.4 Discussion

Specific Aim 1 was designed to standardize the use of the DMOS-IROC as the optical CT scanner for PRESAGE<sup>®</sup> dosimeters at IROC-Houston. A Standard Operating Procedure (SOP) was

developed to assist users in analysis by allowing for the conditions of the imaging to be excluded from any inconsistencies in the data. Various combinations of the variables associated with use of the optical CT were optimized for coverage of the phantom and dynamic range of the output by selection of flood and dark fields. Additional systematic errors such as motor position were identified and implemented in the SOP. The camera and light source settings were set for the duration of experiments. Reconstruction methods were finalized for different sizes of dosimeters to ensure consistency of analysis. The following discusses each section in detail.

#### ***2.4.1 Light Source Physical Setting***

The flood field for this scanner has a region of low intensity in the center. Over time we have tried to correct this by changing the light source itself, switching diffusers and varying positioning of both the light source and diffuser respect to one another and the telecentric lens. The current field is a compromise between flooding the camera with the maximum amount of light in the corners of the largest FOV to maximize the usable FOV for the tank. Losing the edges of the FOV does limit our dosimeter size down from the maximum size of our tank. At this time this limitation has not been an issue.

Refractive index fluid should not affect the flood field image but over time our floods do change. We believe a small amount of dye from our seal at the base of the tank connecting the rotating stage to the motor is coloring the fluid and changing the base optical density. As multiple users are changing the matching fluid composition for different batches of dosimeters this discoloration is difficult to track. When the dynamic range is no longer useful, the matching fluid is completely replaced with new, un-dyed chemicals. Observing the change in flood fields estimates when the changeover must happen. Major changes to the scanner, including fluid change, must be done when no users are between a pre and post scan.

#### **2.4.2 *Camera Field of View***

The user defined camera FOV and consequently the center of rotation for reconstruction was successfully implemented in our group. Each dosimeter that does not fit in a pre-defined FOV is imaged and the center of rotation is documented in a universal spreadsheet each user accesses from the DMOS-IROC computer. This system has increased reproducibility as the center of rotation input for a certain size dosimeter is not user-dependent.

#### **2.4.3 *DMOS-IROC Quality Control***

The checklist for quality control has decreased image acquisition errors and prevented scanner malfunctions. With several users in the lab the quality control ensures that from user to user the system is properly functioning and the flood image is not drifting. A drifting flood image can disrupt an experiment if the flood changes from pre to post scan minutely. On a larger scale a narrowing dynamic range might not be caught until a user cannot image an irradiated dosimeter at a dose expected to be within range for the optical CT.

#### **2.4.4 *Projection Images***

In this experiment the number of projection images was changed until an acceptable balance between acquisition time and signal to noise ratio was reached. The time limiting factor in imaging and reconstruction of a dosimeter is acquiring the projection images. For example, the standard scan defined in this study (8 images averaged for 360 projections with a 1 degree rotation) imaged a dosimeter in less than 15 minutes. In total, with the correct matching index fluid, a dosimeter could be imaged and reconstructed in 20 to 25 minutes total. For studies requiring multiple irradiations for reproducibility, a short imaging time was needed to keep the signal from the dosimeter comparable. Literature has demonstrated for PRESAGE<sup>®</sup> the dose response changes over the time and can increase rapidly in the first few hours post-irradiation (18, 20). By minimizing the imaging time multiple dosimeters can be directly compared. Also, for a remote facility the shorter imaging times

can increase the number of dosimeters that are imaged in a workday and can increase productivity in a busy quality assurance program.

With this investigation completed we could begin to irradiate phantoms and determine the change in optical density in a consistent fashion.



## Chapter 3 - Specific Aim 2

### 3.1 Rationale

The second specific aim was to assess the capability of PRESAGE<sup>®</sup> dosimeters for remote quality assurance. IROC-Houston operates a remote quality assurance program that includes a sizeable mail out anthropomorphic phantom program. PRESAGE<sup>®</sup> would be an excellent addition to this program to provide three dimensional data for the only “end to end” in IROC-Houston’s program (38). For this test to be successful, the PRESAGE<sup>®</sup> dosimeters need to withstand the unique conditions remote dosimetry entails. These conditions include using a single batch for multiple phantoms (ordering one large batch to fulfill several phantom shipments at a time), independence from temperature variations due to shipping and the time elapse from manufacturing to final analysis inherent in remote dosimetry.

The second specific aim was separated into four sections:

- Creating a dose calibration scheme
- Determining the age dependence of the dosimeter
- Determining the temperature dependence of the dosimeter
- Determining the effect of the readout procedure

### 3.2 Methods

#### 3.2.1 Dose Calibrations

Dose calibrations had to be performed for every batch of dosimeters received as previously mentioned in the introduction. The batches varied from one to 10 dosimeters. PRESAGE<sup>®</sup> calibration curves are approximately linear (16) and only three or four dose points were necessary to find the curve. Two methodologies for dose calibrations were examined. One method used a large cylindrical dosimeter similar to a head and neck phantom dosimeter (9 cm diameter by 6 cm height)

while the second method used cuvettes (1 cm x 1 cm by 4 cm container of PRESAGE<sup>®</sup> seen in Figure 3-3). Large volume dosimeters and cuvettes have different cure rates during manufacturing and there is some concern this might cause a change in dose sensitivity (39). Cuvettes are read out using a Genesys 20 Visible Spectrophotometer (Thermo Scientific, Philadelphia PA) but there is no equivalent for a large volume dosimeter. A relative dose measurement using film was devised to measure absorbed dose.

A film phantom (shown in Figure 3-1) was created by cutting a cylinder of PRESAGE<sup>®</sup> dosimeter material into three pieces. By using PRESAGE<sup>®</sup> in place of solid water phantom material a correction factor was not needed (40). The pieces were labeled and marked for orientation. The top piece was  $1.67 \pm 0.05$  cm while the thickness of the middle piece was  $1.76 \pm 0.05$  cm. Three pieces of Gafchromic EBT2 film were used for the irradiations. One piece of film was taped to the top of the dosimeter, one piece between the top and middle sections, and one piece between the middle and base sections. An example of the film is shown in Figure 3-2.



**Figure 3-1: The film phantom for dose calibrations was created from a used PRESAGE<sup>®</sup> dosimeter. Film was sandwiched between the two levels and compared to a dosimeter from the batch of PRESAGE<sup>®</sup> being calibrated.**

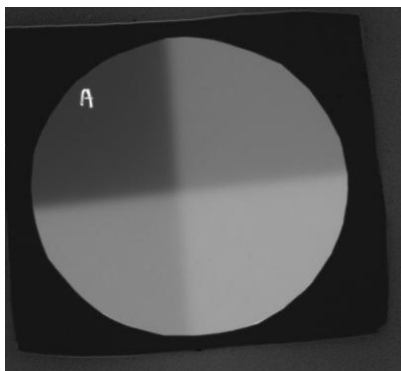


**Figure 3-2: An example of a film irradiated with overlapping dose areas which created 4 dose levels for the calibration curve.**

The film was cut to fit the shape of the cut dosimeter. This PRESAGE<sup>®</sup>/film dosimeter was placed in a water phantom with 5 cm of water above the surface to the top section. A radiation beam was positioned to treat half of the phantom, and a dose of 1.8 Gy was delivered to the level of the uppermost film. The collimator was rotated 90° and a dose of 4.8 Gy was delivered to half of the phantom. In this manner, four different dose levels were created (see Figure 3-2). Different areas of the dosimeter received different dose levels such that a calibration curve was acquired with 8 dose points. The doses delivered at depths in the dosimeter were also estimated from standard water phantom data and were corrected for the presumed electron density of PRESAGE<sup>®</sup>.

A PRESAGE<sup>®</sup> dosimeter made from Batch 01-13 of 9 cm diameter and 6 cm height was irradiated in exactly the same fashion as the PRESAGE<sup>®</sup>/film phantom. The dosimeter was placed in a water phantom with 5 cm of water above the surface of the dosimeter. Two beams were delivered with a 90° rotation between exposures, so that regions of four dose levels were created. This procedure was followed for each new batch of PRESAGE<sup>®</sup>.

The film batch was calibrated separately from the PRESAGE<sup>®</sup> irradiation. The film was set at  $d_{\max}$  in a 6MV beam with 9 cm of water equivalent plastic as backscatter and 1.5 of water equivalent plastic buildup. The table was raised until the top of the solid water phantom was at 100 cm SSD with a field size of a 35 cm x 35 cm. The machine was programmed to deliver at 600

MU/min at the amounts listed in

Table 3-1.

square	MU
1	50
2	150
3	200
4	250
5	350
6	450
7	550
8	650
9	750
10	950
11	1150
12	1350

**Table 3-1: MU delivered to each film square**

The first set of MUs was delivered, and then the room was entered to remove the corresponding film square. The machine was reset to deliver the MU needed to reach the next level and the corresponding square was removed. This was repeated until twelve pieces of film had been irradiated, one to each of the intended MU settings listed in Table 3-1. One square of film was left unirradiated to serve as background. The dose delivered was calculated by hand using the machine specific output factor of 1.095 for the 35 cm x 35 cm field size.

The film was read on a CCD Microdensitometer between 24 and 36 hours post-irradiation. The film measurements were corrected for the flat field response of the microdensitometer with a field of view of 150 cm<sup>2</sup>. ImageJ (NIH, Bethesda, MD) was used to analyze the film images. The mean value of the center of the film squares was measured 3 times with the average used as the optical density. The dose delivered was then plotted against the measured optical density and a third degree polynomial fit was applied.

MATLAB® was used to analyze the reconstructed dose distribution recorded by the PRESAGE® calibration dosimeter and the mean optical density per cm of the dose regions of PRESAGE® in the planes where the films from the film phantom are located was recorded. The film dose calibration curve was used to convert the film's optical density to dose using IROC-Houston's protocol. The OD measured from the PRESAGE® large volume calibration dosimeter was plotted against the measured film dose to create a linear dose calibration curve.



**Figure 3-3: The high-impact phantom containing a cuvette cutout (left) with cuvettes inserted. A close up of the cuvettes is shown on the right.**

An initial experiment to check the linearity of PRESAGE® was performed using the dose levels listed in Table 3-2 to follow the film dose levels as closely as possible. Cuvettes with a volume of 1 cm x 1 cm x 4 cm and containing PRESAGE® of batch 10-12 were irradiated in high impact polystyrene. A cutout to contain 4 cuvettes was sandwiched between slabs of solid water to allow for 1.5 cm buildup and 9 cm backscatter placed in a 35 cm x 35 cm field size. The absorption of the material was read using a Genesys 20 Visible Spectrophotometer prior to and post irradiation and the change in absorption per cm was compared to the dose delivered to the center of the cuvette to calculate the PRESAGE® calibration. Readings were taken 3 times for each cuvette and the average reading was recorded.

One cuvette was irradiated to each dose level. Two additional cuvettes were irradiated to two of the originally-selected dose levels (450 MU and 650 MU) to test reproducibility. The dose

was calculated from the MU delivered and the change in optical density was plotted versus the dose delivered.

<b>Cuvette #</b>	<b>Cuvette MU</b>
<b>1</b>	50
<b>2</b>	150
<b>3</b>	200
<b>4</b>	250
<b>5</b>	350
<b>6</b>	450
<b>7</b>	550
<b>8</b>	650
<b>9</b>	750
<b>10</b>	850
<b>11</b>	650
<b>12</b>	450

**Table 3-2: MU delivered to 12 cuvette study**

A comparison between large volume and cuvette calibration was performed using a single batch of dosimeters. For this study, dosimeters of Batch 01-13 were used. A large-volume PRESAGE<sup>®</sup> dosimeter of dimensions 9 cm diameter by 6 cm height was irradiated in the same fashion, using two beams with a 90° rotation, as was described above. The MU delivered to the large volume dosimeter were 0 MU, 200 MU , 650 MU and 850 MU in each respective quadrant. The cuvettes received a similar MU delivery with 50 MU, 200 MU, 650 MU and 850 MU. The procedure was detailed above. Each dose was calculated and plotted together to compare the slope of the respective measured calibrations. The difference was then quantified.

### **3.2.2 Age and Temperature Dependence**

One concern with remote dosimetry is whether it is feasible to have physicists at other sites store dosimeters under the same conditions as at IROC-Houston. The loss of control over the storage and handling conditions at the site to be evaluated can affect the results. This experiment was done

with two separate batches of PRESAGE<sup>®</sup> and tested the effects of different storage temperatures, extreme shipping temperatures and extreme irradiation temperatures using dosimeters which were recently manufactured and dosimeters manufactured 3 or 4 months before irradiation. Each separate experiment was analyzed as a standalone data set and as an overall dataset (where applicable).

The first experiment tested the difference in measured change in optical density from dosimeters that were irradiated in the same conditions but stored after irradiation at either at 3°C or room temperature ( $\approx 22.7^\circ\text{C}$ ). Upon receipt from the manufacturer, the dosimeters were placed in a refrigerator for storage prior to irradiation. Each dosimeter was irradiated under the same conditions at different times: within 1 week of receipt from the manufacturer and at 3.5 months post receipt from the manufacturer. The dosimeters were irradiated in a water phantom using a Varian 2100 machine (Varian Medical Systems, Pal Alto, CA.) The machine was set to 400 monitor units at 6 MV to irradiate the center of the dosimeter with the gantry set at  $270^\circ$ , 10 cm of water proximal to the dosimeter and 9.5 cm of backscatter. Up until irradiation the dosimeters were stored at 3° and brought to room temperature for the irradiation. After irradiation all dosimeters were imaged for a baseline reading. One dosimeter was returned to a cold environment (labeled “SC” for stored cold) and the second dosimeter was left at room temperature (labeled “SR” for stored at room temperature.)



**Figure 3-4: Set up for storage and temperature irradiations.**

The dosimeters were imaged at room temperature and at varying times over several weeks with the time noted in days since irradiation. The imaging system was the DMOS-IROC (22) and the scanning procedure was described in more detail in Chapter 2. All dosimeters were imaged with  $1^\circ$  rotation for 360 steps with a flood and dark correction. Reconstruction was done with a 2 mm slice width and a Hamming filter. Every dosimeter was imaged prior to irradiation (referred to as a pre-scan). The pre-scan and post-scan (considered to be any imaging done post-irradiation) were subtracted prior to full reconstruction. This eliminated un-irradiated sections of the dosimeter from the final measured dose volume. The center slice of the dosimeter was measured in MATLAB and the mean change in optical density was plotted against the time from irradiation.

For remote dosimetry, shipping is of great concern for the stability of the dose measurement. It has been shown that storage in cold temperatures minimizes post-irradiation change in dose response and increase the stability of the dosimeter (20). Four dosimeters were used in this study. Two were exposed to extreme cold conditions ( $\approx -18^\circ\text{C}$ ) by staying in the freezer for 24 hours while the other 2 were exposed to extreme hot (maximum  $66^\circ\text{C}$ ) by staying on the dashboard of a car



parked in the sun for 24 hours. Two dosimeters experienced the extreme condition prior to irradiation (one to extreme cold conditions and one to extreme hot conditions) while the other two dosimeters were exposed to the extreme conditions post irradiation. The stability of the reading was measured over time with the dosimeters stored at 3°C between readings. All irradiations and readings were conducted at room temperature. The irradiation and imaging settings were the same as stated above.



**Figure 3-5: Dosimeters being brought to extreme cold or hot for irradiation. The equilibration was done in a water bath for irradiation.**

The last condition investigated in the temperature study was the effect on response of the temperature of the dosimeters during irradiation. This experiment simulated the situation when an irradiation is performed without a dosimeter being brought to room temperature. This could occur with an irradiation shortly after receiving a dosimeter or when removing a properly stored dosimeter for an onsite irradiation.

Three dosimeters were used for this experiment. All dosimeters were stored at 3°C upon receipt from the manufacturer and between every post scan. The dosimeters were pre-scanned and one was placed in ice water ( $\approx 3.5^{\circ}\text{C}$ ), a second wrapped in hot packs prior to being placed in hot water ( $\approx 35.6^{\circ}\text{C}$ ) as see in Figure 3-5, and the third dosimeter was kept at room temperature. All three

irradiations were performed as described above. All dosimeters were then brought to room temperature and post-scanned using the same settings described previously. The dosimeters were scanned repeatedly over about 25 days to record the changing OD over time. The same post-scan settings were used as described above and the dosimeters were at 3°C and brought to room temperature for every scan.

### **3.2.3 Readout Procedure**

Over the course of the extended time experiments the dosimeters were placed in a 633±5 nm wavelength for 16 – 18 scans (including pre-scans). Each scan exposed the dosimeter to 15 minutes of red light at minimum. This experiment evaluated the effect of exposure to the red wavelength. An unirradiated dosimeter was placed in the DMOS-IROC and the pixel value through the center of the dosimeter was recorded over 5 hours to record any change in OD due to the scanning procedure.

## **3.3 Results**

### **3.3.1 Dose Calibrations**

The film calibration results are shown in Figure 3-6. The film demonstrated a response to dose that can be described with a polynomial as  $OD = 0.0004x^3 - 0.0137x^2 + 0.1542x$  where x is the dose delivered in Gy. Large volume PRESAGE® calibrations were performed for all phantom experiments. These results were for PRESAGE® Batch 01-13 which was used to compare to the cuvette calibration technique. Three films were irradiated at each dose level. The largest standard deviation was observed at 7.1Gy and was 0.003 OD or 0.5 %.

OD

**Figure 3-6: Film Calibration for film used in PRESAGE® calibration phantom and HN phantom irradiations. Error bars indicate one standard deviation.**

The PRESAGE® “large volume” calibration was performed with three dosimeters of Batch 01-13. The experiment used 2 depths for dose measurements and 8 total dose points. The results are shown in Figure 3-7 where the slope of the dose response curve, determined from 3 repeat measurements, was  $0.0319 \pm 0.015 \Delta OD \cdot Gy^{-1} \cdot cm^{-1}$ . As was described in Section 1.3.1, the response of PRESAGE® is described in terms of an optical attenuation coefficient,  $OD \cdot cm^{-1}$ , to enable construction of a map of OD measurements. The calculated dose estimates varied up to 10% from the film measurements and were not considered reliable for dose calibrations.

$\Delta OD / cm$

**Figure 3-7: PRESAGE<sup>®</sup> Batch 01-13 Dose Response**

The results of the linearity study performed using 12 cuvettes containing PRESAGE<sup>®</sup> from batch 10-12 are shown in Figure 3-8. The slope showed to be linear through almost 10 Gy covering any hot spot anticipated in QA phantom studies. The cuvettes irradiated to the same dose point at different times were within the uncertainty of the measurement.

$\Delta OD / cm$

**Figure 3-8: 12 Dose Response of Cuvettes Containing PRESAGE<sup>®</sup>**

$\Delta \text{OD} / \text{cm}$ 

**Figure 3-9: Dose Response of Cuvettes Containing PRESAGE® Batch 01-13**

The cuvette calibration of Batch 01-13 (Figure 3-9) measured a dose response curve with a slope, determined from 3 repeat measurements, of  $0.0255 \pm 0.003 \Delta\text{OD} \cdot \text{Gy}^{-1} \cdot \text{cm}^{-1}$ . This differed from the large volume dose by  $0.006 \Delta\text{OD} \cdot \text{Gy}^{-1} \cdot \text{cm}^{-1}$ . The effect of differing slopes is illustrated in Figure 3-10. The steeper slope of the large volume dose response shows a greater sensitivity to dose than the cuvettes. At lower doses, below 4 Gy, the data suggested the two measurements fell within the others' uncertainty. At larger doses, the curves continue to diverge suggesting that the largest dose delivered in a HN phantom study (discussed in greater detail in Specific Aim 3) would not be properly related to  $\text{OD} \cdot \text{cm}^{-1}$  by the cuvette calibration method.

$\Delta$  OD / cm

**Figure 3-10: Batch 01-13 Dose Response Comparison**

### 3.3.2 *Age and Temperature Dependence*

The storage temperature experiment followed 4 dosimeters over approximately 15 to 25 days and is shown in Figure 3-11. The dosimeters stored at colder temperatures showed an increase in OD over time regardless of the age of the dosimeter at irradiation. The dosimeters stored at room temperature showed an initial increase in pixel values followed by a fading of signal. The older dosimeter began to fade near day 4 while the newer dosimeter did not begin to fade until day 11.

$\Delta$  OD / m m

**Figure 3-11: Storage Temperatures with repeated post scans over time.**

$\Delta OD / mm$ 

**Figure 3-12: Temperature changes prior to and post irradiation**

In Figure 3-12 the control dosimeter was the same dosimeter irradiated for the storage experiment described in Figure 3-11 in the previous section and is shown in blue diamonds. Both the dosimeters exposed to freezing temperatures (shown in circles and triangles) and the dosimeter exposed to heat prior to irradiation (depicted in squares) trended well with the control. The dosimeter exposed to heat after irradiation initially agreed with the others but quickly faded off.

 $\Delta OD / mm$ 

**Figure 3-13: Temperature changes at irradiation**

Δ OD / cm

**Figure 3-14: Initial Readout with Varying Irradiation Temperature**

As shown in Figure 3-13, the readings taken on the day of irradiation showed large differences. This is in contrast to the prior experiments shown in Figure 3-12, in which the readings taken on the day of irradiation were all quite similar. All dose response readings for the 3 irradiations rose over time with the smallest amount of change occurring in the dosimeter that was heated during irradiation. This smaller change could be attributed to the dosimeter's higher initial response. In Figure 3-14, the initial readout OD change is compared to the irradiation temperature with measured values (points) and fitted calculations (lines). This display format was chosen to enable a comparison of the temperature dependence of the reaction rates between our dosimeters and the cuvettes used by Skyt *et. al.* (41).

### 3.3.3 Readout Procedure

A dosimeter that had been irradiated with a simple 4 cm square field was set in the DMOS-IROC tank and a single live projection image was observed. The DMOS-IROC camera reported a pixel value reading of 2400 at the exact center of the dosimeter. The pixel value is related to the light intensity received by the CCD camera and, for dose distribution reconstructions, would be used to calculate the OD and subsequently the dose. Pixel value observations were taken at 0.5, 1, 2, 3, 4 and



5 hours and a constant pixel value of 2400 was observed throughout the study. Data were not taken after 5 hours to avoid prolonged exposure to the DMOS-IROC light source from causing OD changes to occur even in a darkened environment. The 5 hour elapsed time still encompassed the total time a dosimeter would be exposed to the DMOS-IROC light during a scanning procedure and through repeat scans taken to measure change in dose response over time.

## 3.4 Discussion

### 3.4.1 Dose Calibrations

Two dose calibration schemes were tested in this section: a calibration using 8 dose levels measured in a large-volume dosimeter and a calibration using 4 small volume cuvette dosimeters. The two methodologies both demonstrated linear slopes (expected for PRESAGE<sup>®</sup>) and gave dose calibrations with slopes within  $0.006 \Delta OD \cdot Gy^{-1} \cdot cm^{-1}$  when compared directly using the same batch. Investigations for large volume and cuvette calibrations were made due to possible complications due to differences in response and methodologies.

For the large volume dosimeter the doses delivered at depths in the dosimeter were estimated from standard water phantom data and were corrected for the presumed electron density of PRESAGE<sup>®</sup>. As an alternative procedure, doses were measured with film. The dose measured with film was then used to calculate the PRESAGE<sup>®</sup>  $\Delta OD \cdot Gy^{-1} \cdot cm^{-1}$ . This added step introduced the uncertainty of the film measurement, determined to be less than 1% in Section 3.3.1, to the overall dose calibration. However, the doses estimated from standard water phantom data were considered less reliable because, at the time of this experiment, the radiological properties of PRESAGE<sup>®</sup> were not known with sufficient confidence.

The readout for the large volume dosimeter was done with the DMOS-IROC while a spectrophotometer was used to analyze the cuvettes. While theoretically the same wavelength of light was used for both the DMOS-IROC and the spectrophotometer, differences in the light

production (LED verses prism) could have affected the OD readout and induced the differences seen in Figure 3-10. Vidovic *et. al.* directly compared a smaller version of the DMOS-IROC (with 50 micron resolution called the DMicroOS using an 633 nm LED light source) to a spectrophotometer reading (set to 633 nm) with a molded cylindrical PRESAGE<sup>®</sup> that fit within both instruments (42). This study found a difference of 0.88% in sensitivity suggesting the modality (and the light source) used for optical readout does not greatly affect the OD/cm measurement. A similar study with molded cylinders would need to be performed to confirm this finding in our larger DMOS-IROC scanner. The change in resolution is not expected to change the OD in simple open field irradiations used for dose calibration and indicates the difference in sensitivity we found is more likely do to the volume differences.

The cuvettes were read using a spectrophotometer whose settings do not change between pre and post scanning. As there is no fluid involved it is easier for the user to control the measurement environment. The cuvettes identical sizing allowed for the creation of a solid water cutout allowing for a solid full scatter phantom for dose calibration. There is some discussion in the literature that the volume of PRESAGE<sup>®</sup> might affect the OD change from radiation (18, 43, 44). The strength of the lattice due to differences in cure rates for different volumes is suspected but the full reasoning at this time is unknown and beyond the scope of this project (45). While it is currently common practice in the community to use cuvettes for calibration of a batch of dosimeters, more investigation needs to be performed in volume differences in dose response to use this dosimeter as an absolute dosimeter.

For this project the ability to use cuvettes was not available until near the end of measurements. As the phantom measurements were all relative and scaled to TLD point dose measurements, an absolute calibration was not necessary. The large volume calibration was chosen as a starting point for all dose calibrations for consistency over the course of the investigation and as the most accurate method due to the volume difference in the large dosimeter and the cuvettes. Should IROC-Houston move forward with relative PRESAGE<sup>®</sup> measurements investigation towards

the use of the cuvette calibration is advised. If lower doses are used for phantom irradiations the sensitivity difference in calibration methodologies might not affect the final dose readout. The cuvette calibration method is less expensive and a less time consuming process for a batch by batch dose calibration. Also, for different anthropomorphic phantoms the shape of the dosimeter could change away from the simple cylinder and the cuvette calibration might become the more reliable method for calibration. If there is a known suspicion that the volume of the dosimeter changes the sensitivity, the geometry (i.e. a long dosimeter versus a short dosimeter with different diameters) could also change the curing rate and the sensitivity for the dosimeter. For absolute measurements more investigation will be needed of potential volume effects.

#### ***3.4.2 Age and Temperature Dependence***

Remote dosimetry depends on having dosimeters reliably record and retain dose and dose distributions for a certain period of time after irradiation. Ideally, the recorded dose would not change once the dosimeter has fully developed. PRESAGE<sup>®</sup> has been characterized to have increasing signal followed by fading over time as shown in Section 3.3.2. With the dosimeter used as a relative dosimeter and the dose scaled to a point, a change of signal can be acceptable if that change can be characterized. In all situations, a dosimeter stored in a cold environment did not show any signal fading. The dosimeters stored at room temperature showed measurable fading after a certain time point (Figure 3-11). This point was dependent on the age of the dosimeter at the time of irradiation. Remarkably, this was the only time in this study an older dosimeter showed significant difference from a newer dosimeter. Aged dosimeters record dose correctly in a simple open field environment. All measurements in this study were across a center slice excluding the outer perimeter and further investigation is needed for doses closer to the edges of the dosimeters. Dosimeters need to be manufactured close to irradiation date and not stored for months prior to sending them out for maximum reliability.

Temperatures can be controlled in lab settings but are almost unavoidable with remote dosimetry. The greatest concern is the temperature variability the dosimeter might be exposed to during the shipping process. Four dosimeters were exposed to extreme temperature situations prior to and post irradiation to test for readout stability. All results except those from the dosimeter that was heated post irradiation were comparable to the results from the control dosimeter. The dosimeter heated post irradiation were comparable to the results from the control dosimeter. The dosimeter heated after irradiation (which could reach 66°C) immediately faded and stayed near 0.012 OD / mm for the duration of scans. The initial reading taken immediately post-irradiation was performed prior to heating the dosimeter showing the dosimeter was correctly irradiated to the same dose as the other dosimeters. Shipping dosimeters should be done with a priority method to avoid any delays that could allow the dosimeter to reach a high internal temperature on the return trip to IROC-Houston. Methods of temperature gauge should be researched prior to implementing remote dosimetry to ensure the package never reached a critically high temperature. This could include a piece of film or other small thermally reactive material. IROC-Houston anthropomorphic phantom cases are well insulated and should not reach the critically high temperatures used in this study. But, any use of the mail-out system to send a stand- alone dosimeter would need to be closely monitored and/or well-insulated for the return trip.

The temperature of the dosimeter at irradiation also results in a different reading for each dosimeter. The change in response over time was measurably different in the first 3 to 4 days and then response increase appeared to continue at the same rate regardless of irradiation temperature. By using PRESAGE<sup>®</sup> as a relative dosimeter, the uncertainty in dose response can be lessened by requesting all dosimeters are irradiated at room temperature and ensuring the calibration dosimeter is also irradiated at room temperature.

More studies are needed to characterize the fading point (in time) of different aged dosimeters. Due to the cost of the dosimeters and limited amount of dosimeters that can be made from a single batch this is a difficult prospect for the large volumes. As every batch of dosimeters

potentially has a different sensitivity it can be assumed the fading characterization could also change. To characterize fading over time in large volumes would be a separate project. Skyt *et. al.* (41) have performed a similar study using cuvettes. Figure 3-14 was the only direct comparison made between the two studies. With different dose prescriptions and PRESAGE<sup>®</sup> batches the data was not expected to exactly reproduce. The large volume OD change with temperature trended well with the published cuvette results. The cuvette data showed the same trend of dosimeters stored at higher temperatures increasing in OD until near the 10 day mark and then decreasing. Lower temperatures continued to increase without reaching a threshold. This corresponded with the new dosimeters tracked in Figure 3-11. The older dosimeter began to fade much sooner (near day 3) implying dosimeters were better used as close to manufacturing as possible. If dosimeters are returned prior to the fading point they can be readout with a corresponding calibration. Otherwise, the fading of dosimeters would need to be characterized to know if the intrabatch fading is equal. The calibration dosimeters should be kept in the same thermal situation as the experimental dosimeter to minimize differences. While PRESAGE<sup>®</sup> is not yet capable to be an absolute dosimeter, keeping the calibration close to the experimental dosimeter is good practice to minimize the relative correction as the field moves towards using 3D dosimeters for absolute dose measurements (28, 43, 46).

Volume effects of PRESAGE<sup>®</sup> response have been discussed in several studies (41, 43) questioning if there are differences due to the different rates in curing and polymer strength and how great an impact this could make on measurements. This study investigated whether using a larger volume greatly affected the response characterized in cuvettes. Cuvettes were analyzed using a spectrophotometer as opposed to optical CT introducing a different light spectrum and no reliance on a CCD camera. Any of these variabilities could cause a discrepancy making cuvettes unreliable for characterizing large volume PRESAGE<sup>®</sup>. This study analyzed the volume appropriate for remote phantom dosimetry in the same optical setup used for phantom studies to reduce readout variabilities not induced by temperature or time. The data's agreement with cuvette data was acceptable to make

the case for using cuvettes to model the large volume dose response at doses below 4 Gy. This further backed up the recommendation made earlier to continue future dose calibration with the cuvette method if the dose prescription is lowered. As formulations mature and characterizations need to be re-examined for validity, the cuvette method is less time consuming and could carry the majority of the data though a larger volume dataset should also be analyzed to verify the volume of the dosimeter is not affecting the dose readouts.

### **3.4.3 *Readout Procedure***

To ensure none of the OD readouts from the age experiments were falsely increased by the red light exposure a measurement of the OD change of a dosimeter not exposed to ultraviolet or ionizing radiation was performed. There was no change measured in 5 hours of constant exposure that exceeded the time any of the dosimeters in the former experiments were placed in the scanning tank. This was expected and removed the need to account for red light exposure in the previous results. In most situations a dosimeter would never reach the 5 hour mark in a tank and this experiment was solely to validate the age experiments where multiple post-scans were necessary.

## Chapter 4 – Specific Aim 3

### 4.1 Rationale

As treatment plans become more complex, it is increasingly difficult to assure the intended calculated dose is being delivered correctly. Using a volumetric dosimeter in quality assurance for complex treatment plans gives the user a large increase in information as compared to planar films. This means that by using the 3D measurement data set, more robust comparisons to the TPS can be made. Currently, IROC-Houston uses film planes and TLD to evaluate phantom irradiations. The film measurements are analyzed using a 2D gamma with 7%/4mm passing criteria (discussed in more detail in the introduction). Literature has shown this may or may not be an appropriate passing criterion for a 3D dataset (27). As part of this specific aim, various gamma constraints were calculated to identify a relevant constraint for properly delivered treatment plans using 3D dose measurements.

The previous experiments were designed to test the optical CT scanner and the PRESAGE<sup>®</sup> dosimeter separately. This section uses the system as a whole. Treatment plans were created which ranged in complexity from simple open fields to complex, clinically relevant plans for IMRT. Each plan was compared against film and TLD measurements and the TPS. Gamma index analyses with various constraints were applied for comparison to assist in choosing appropriate constraints for evaluation.

The third specific aim is separated into three sections:

- Irradiating the phantom with open field plans
- Irradiating the field with IMRT plan
- Modifying gamma analysis constraints

## 4.2 Methods

### 4.2.1 Open field plan

To begin, simple open field treatment plans were created using the IROC-Houston HN phantom to confirm that the dosimetry system was able to verify the TPS prior to working on complex plans. The HN phantom was developed by IROC-Houston to credential institutions participating in certain RTOG clinical trials (47). The film/TLD insert contains 8 TLD capsules and 2 planes of Gafchromic EBT2 film. Figure 4-1 shows the cylindrical insert used for imaging and an axial CT slice with labeled structures in the film plane. The phantom was designed with two primary target volumes (PTV) and a critical structure to avoid. Eight TLD capsules were placed in the insert: 4 in the primary PTV, 2 in the secondary PTV and 2 in the critical structure. Half of the TLDS were 2 mm inferior to the axial film and half of the TLDs were 2 mm superior to the axial film. A piece of film bisected the primary PTV. A second insert was used to hold a PRESAGE<sup>®</sup> dosimeter in the same area as the imaging insert. Figure 4-2 and Figure 4-3 show the separate inserts with contours from the TPS.

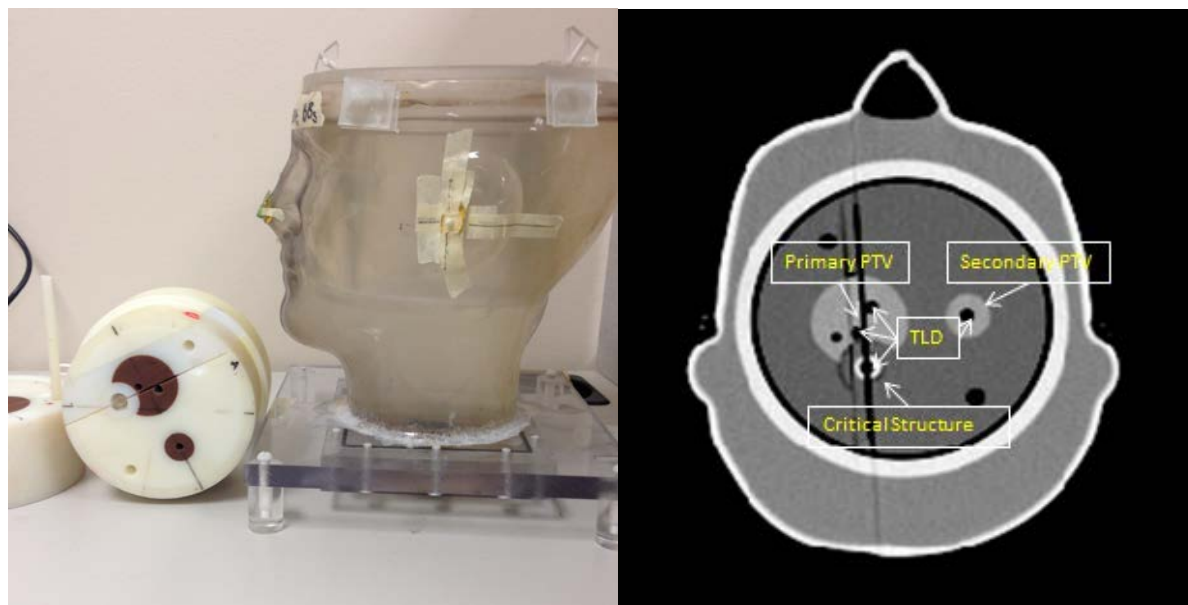


**Figure 4-1:** The HN phantom and imaging insert (left). A CT slice of the imaging insert with labeled structures (right).



The HN phantom was scanned using a GE LightSpeed RT16 CT scanner. One scan was performed using a film/TLD insert (Figure 4-2) and a second scan was performed using the PRESAGE<sup>®</sup> insert (Figure 4-3). Both scans were imported into the Pinnacle<sup>3</sup> TPS (version 9; Philips Healthcare, Fitchburg, WI). Localization was performed with 3 BBs: two placed in the ears and one placed on the tip of the nose. Internal structures and the TLD capsules were contoured. These contours were used for every treatment plan evaluated in this study.

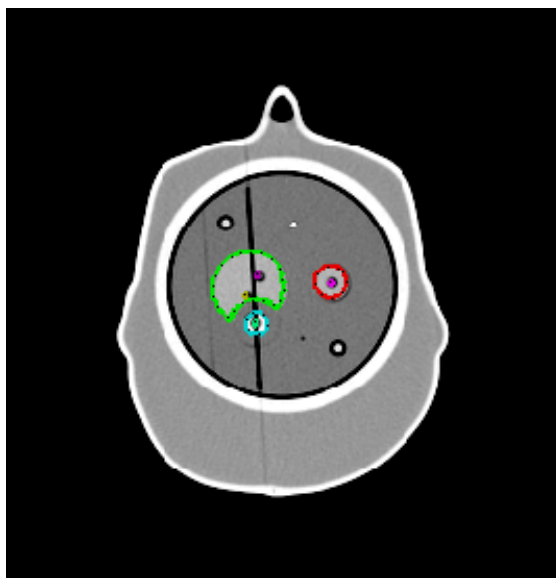


**Figure 4-2: film/TLD Insert with structures and TLD contoured**

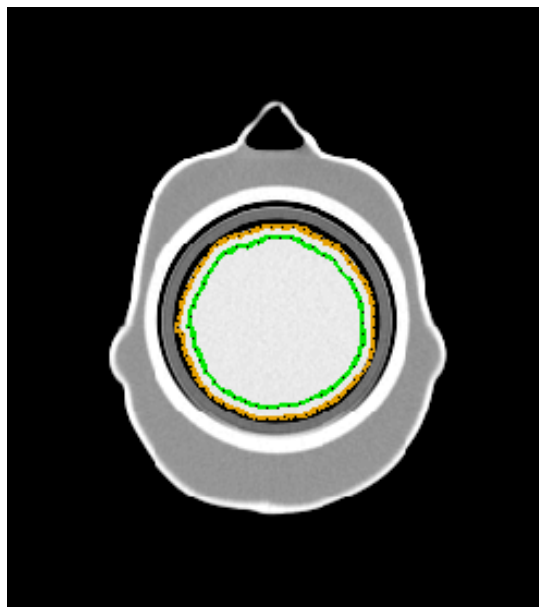


**Figure 4-3: PRESAGE<sup>®</sup> Insert with the dosimeter surface contoured (orange) and a second contour drawn 5 mm inside the surface of the dosimeter (green)**

A single plan was created and the dose distribution was calculated using the two sets of CT scans. The plan created on the film/TLD insert was moved to the CT image set of the PRESAGE<sup>®</sup> insert for analysis. The plan had a 2 beam configuration: anterior-posterior (AP) and right-lateral (RL) referred to as the APRL plan from here on. This plan prescription delivered 500 cGy to the isocenter delivered with 60% (361 MU) of the dose in the AP direction and 40% (226 MU) in the RL direction with the phantom aligned to the BBs. These plans were exported and used for analysis with the PRESAGE<sup>®</sup> irradiations.



**Figure 4-4: Phantom setup with laser alignment to BBs**

Six irradiations were performed using the APRL plan using a Varian 600 machine. The film/TLD insert was irradiated 3 times using 3 sets of dosimeters. The PRESAGE<sup>®</sup> insert was also irradiated 3 separate times with 3 separate dosimeters. The phantom was aligned on the treatment table using the alignment BBs as shown in Figure 4-4. The plan was delivered in QA mode through the MosaiQ delivery system (Elekta AB, Stockholm, Sweden). The film/TLD and PRESAGE<sup>®</sup> dosimeters were all irradiated in the same session.

A large volume PRESAGE<sup>®</sup> calibration (methodology described in detail in Section 3.2.1) was performed with MU inputs of 0, 300, 600 and 900.

The TLDs were read 15 days post-irradiation. After calculating the dose (described in detail in Section 1.4.1) the ratio for measured dose versus calculated dose from the TPS was taken. A value between 0.95 and 1.05 was considered passing. Reproducibility was checked using the coefficient of variance and a value less than 3% was considered acceptable for the purpose of this project. Statistical significance was checked using a one-sample t-test with  $\alpha = 0.05$  as the significance level

and a null hypothesis of  $\mu_0 = 0.949$ . The Excel function TDIST was used to calculate the p-value (the probability of rejecting the null hypothesis), which needed to be less than 0.05 to be statistically significant.

The films were scanned 2 days post-irradiation with a CCD Microdensitometer for Radiochromic Film (Model CCD100 Photelectron Corporation, Lexington, MA). An un-irradiated piece of film from the same batch was scanned to correct for background dose and non-uniformities in the densitometer response. A 1 cm grid was imaged for spatial calibration. The irradiated films were imaged, spatially calibrated and corrected before being saved as FIT files. The film image file was then loaded into IROC- Houston internal software and registered to the phantom plan using registration pinpricks that were applied when the film was first loaded into the phantom. The dose calibration curve for the film was applied and the dose was scaled relative to the TLD readings in the PTV. The film was registered to the treatment plan calculated using the film/TLD insert CT scan. Three dose profiles were taken and their locations are shown in Figure 4-5. Two profiles were taken on the axial film: a right-left profile bisecting the secondary PTV structure and PTV and a superior-inferior profile bisecting the PTV. The third profile was also a superior-inferior profile bisecting the PTV taken on the sagittal film. The 2D gamma analysis at 5%/3mm distance to agreement (DTA) was performed on both films over the entire film area. Pinpricks and the separation area for the sagittal film were removed from the calculation area to account for user-generated discrepancies.

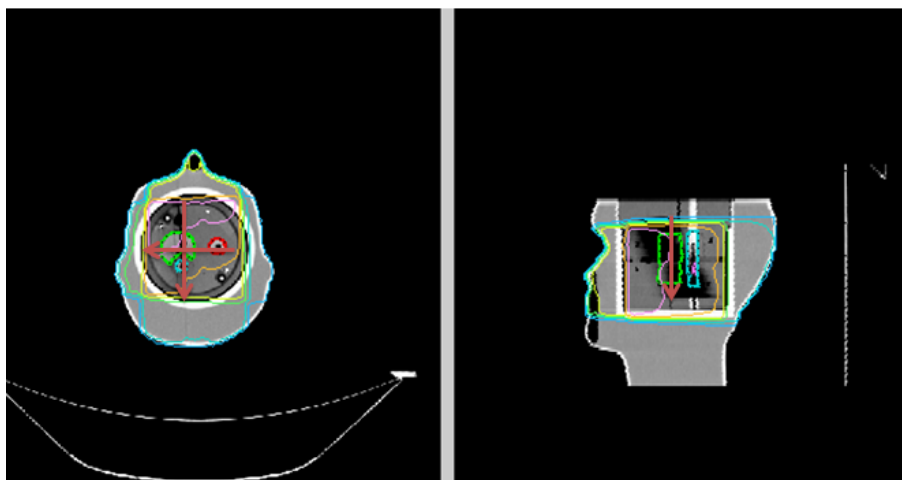


**Figure 4-5: Film Profile locations**

The PRESAGE<sup>®</sup> dosimeter was scanned with the DMOS as described in section 2.3.2 using the settings in

Table 4-1.

<b>Scan Settings</b>	
<b>Degrees Rotation</b>	1
<b>Number Projections</b>	360
<b>Number Images Averaged</b>	8
<b>Flood/Dark Image Average</b>	200
<b>Reconstruction Settings</b>	
<b>Voxel Edge (mm)</b>	1
<b>Center of Rotation</b>	585
<b>Filter</b>	Ram Lak

**Table 4-1: DMOS Settings for HN Phantom Irradiations**

The PRESAGE<sup>®</sup> optical density cube was uploaded to a CERR file containing the treatment plans calculated on both inserts. At this point, the CERR file contained the treatment plan and contours from the film/TLD insert, the treatment plan calculated using the PRESAGE<sup>®</sup> insert and the change in optical density from the PRESAGE<sup>®</sup> dosimeter. The optical density files were initially

calibrated using the large volume dose calibration curve for the batch. The image fusion function was used to fuse the PRESAGE<sup>®</sup> dose reconstruction to the PRESAGE<sup>®</sup> scan. The dose at each TLD point was recorded and compared to the average measured TLD dose for the irradiation and the PRESAGE<sup>®</sup> dose was scaled a second time to the measured dose.

<b>Dimension</b>	<b>Coordinates</b>
<b>Sagittal (x-axis)</b>	-1.35 cm
<b>Coronal (y-axis)</b>	-11.80 cm
<b>Axial (z-axis)</b>	-25.99 cm

**Table 4-2: CERR coordinates for 2D Gamma Comparison**

Dose profiles were taken along the same 3 locations as the film (Figure 4-5) for comparison. A 2D gamma at 5%/3mm was taken in the axial and sagittal planes matching the film planes and also the coronal plane through the center of the PTV (described in Table 4-2). A 3D gamma at 5%/3mm was taken for the whole PRESAGE<sup>®</sup> dosimeter with a 5 mm contracted contour to reduce the effect of the edge artifact.

#### 4.2.2 IMRT Plan

A 9 beam IMRT plan was created using the dose prescription in Table 4-3. This prescription was modified from the current instructions for the HN phantom provided by IROC-Houston to institutions wishing to be credentialed for clinical trials using the HN phantom. The secondary PTV was changed to the “parotid” and the dose was lowered to coincide with dose values quoted by Dijkema *et al* (48). The parotid was added to the plan to provide a normal tissue to predict tumor control in a later study.

<b>Primary PTV</b>	6.6 Gy to at least 95% of the PTV < 1% of the PTV receives < 93% of the prescribed dose.
<b>Parotid</b>	3 Gy to at least 95% of the PTV and
<b>Organ at risk</b>	< 4.5 Gy, maximum dose.
<b>Normal tissue</b>	≤ 110% of the prescribed dose (6.6 Gy).

**Table 4-3: IMRT Dose Prescription**

Six irradiations were performed using the IMRT plan. As stated in the previous section, the film/TLD insert was irradiated 3 times using 3 separate sets of dosimeters and the PRESAGE<sup>®</sup> insert was irradiated 3 separate times using 3 separate dosimeters. The phantom was aligned on the treatment table using the alignment BBs and the treatment plan was delivered in QA mode through the MosaiQ delivery system. The film/TLD and PRESAGE<sup>®</sup> dosimeters were all irradiated in the same session.

A large volume PRESAGE<sup>®</sup> calibration (methodology described in detail in Section 3.2.1) was performed with MU inputs of 0, 200, 650 and 850. The TLDs were read 16 days post-irradiation. At this point the methodology was the same as described for the APRL irradiations.

#### **4.2.3 *Gamma Constraints***

This study was designed to define an appropriate gamma constraint and passing percentage (percentage of pixels passing at a certain constraint) for the PRESAGE<sup>®</sup> dosimeter which has not been defined in literature. Varying gamma constraints allowed a comparison of percentage of passing pixels from different gamma indexes between the different constraint levels and between the different dosimeters. The initial analysis was performed using a gamma constraint of 5%/3mm DTA to test the hypothesis. Two more gamma constraints were studied: 3%/3mm DTA for its prevalence in the clinic (5) and 7%/4mm DTA for its current constraint for IROC credentialing .

The gamma index was calculated as described above in Section 1.5. Additionally, the passing percentage for each contoured structure was recorded.

## 4.3 Results

### 4.3.1 Open Field Results

The average TLD dose from all three trials for the APRL plan is listed in Table 4-4.

<b>TLD Location</b>	<b>Measured Dose (cGy)</b>	<b>Predicted Dose (cGy)</b>	<b>Measured/Predicted Dose</b>	<b>COV</b>
PTV Sup Post	530	528	1.00	0.76%
PTV Inf Post	530	519	1.02	1.48%
PTV Sup Ant	530	526	1.01	1.61%
PTV Inf Ant	533	521	1.02	0.63%
Cord Superior	496	486	1.02	0.67%
Cord Inferior	492	479	1.03	1.37%
Parotid Superior	497	495	1.00	0.43%
Parotid Inferior	496	490	1.01	1.15%

**Table 4-4: Average TLD Results from 3 APRL Irradiations**

The ratios of the measured to predicted doses all range from 1.00 – 1.03 and are within the pass rate of 0.95 – 1.05. The COV values for all TLD are below 3%.



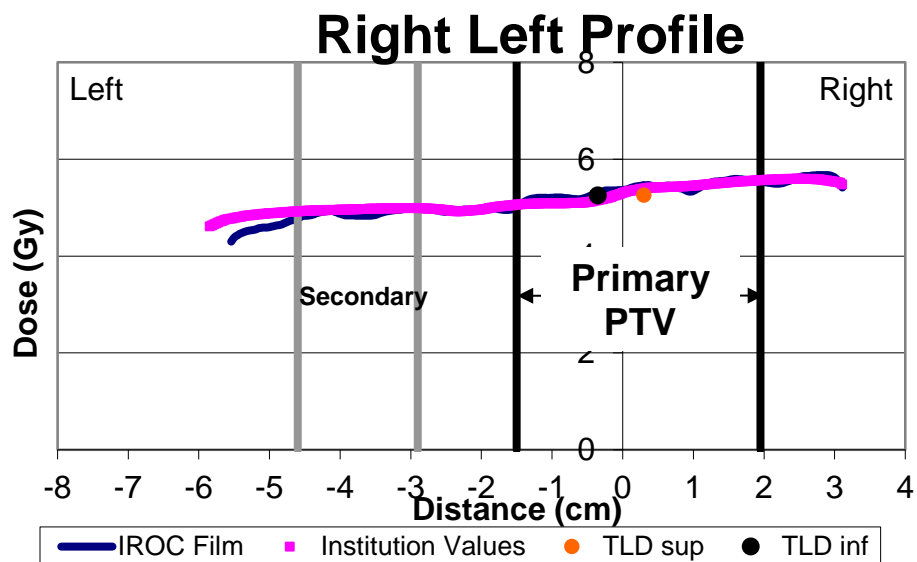


Figure 4-6: Right-Left film profile from Trial 1 of APRL plan

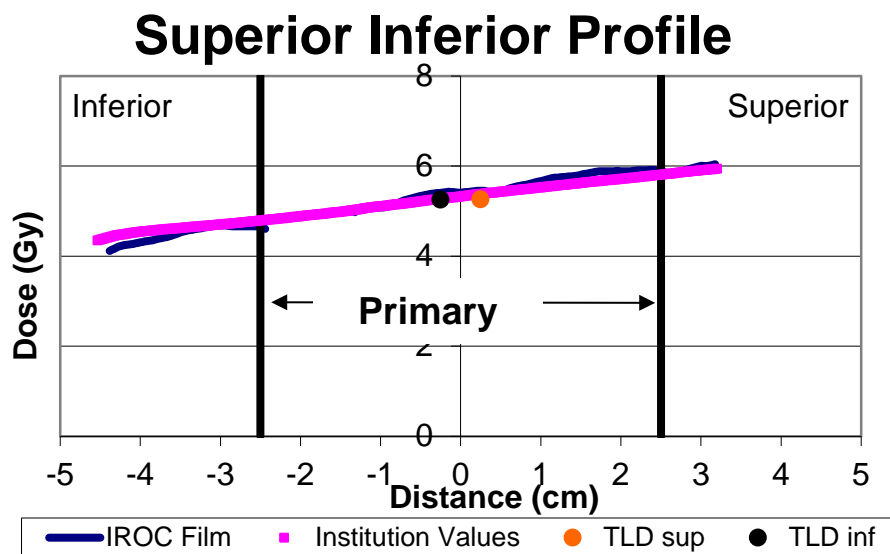
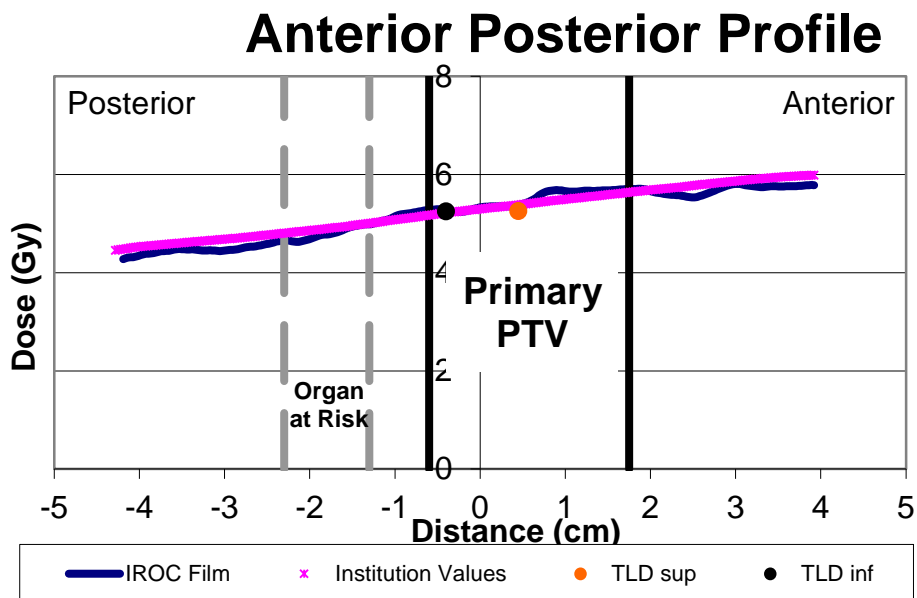
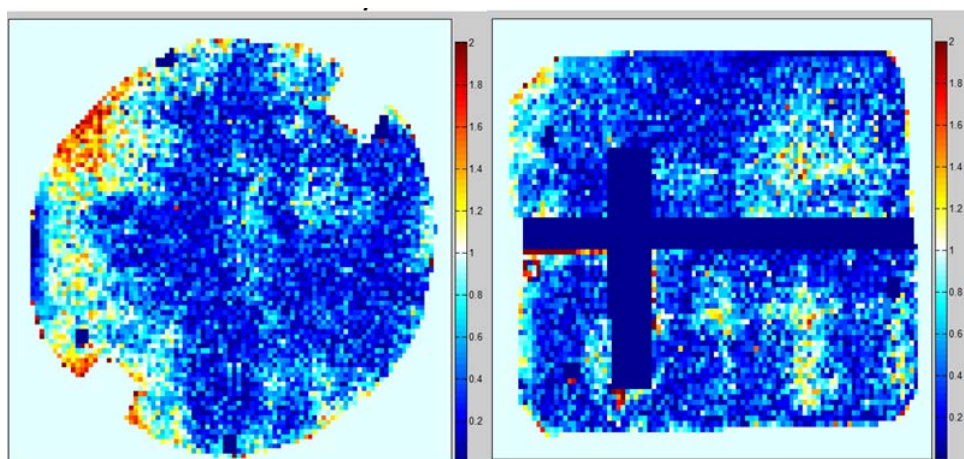


Figure 4-7: Superior-Inferior film profile from Trial 1 of APRL plan



**Figure 4-8: Anterior-Posterior film profile from Trial 1 of APRL plan**

The film profiles taken from trial 1 in the locations shown in Figure 4-5 are displayed in Figure 4-6 through Figure 4-8. The film area was smaller than the radiation field and dose fall off was not measured. Other than a 5% difference at the edge of the RL profile (attributed to pressure marks on the film seen in Figure 4-9) the measured dose stayed within 1% of the calculated values.



**Figure 4-9: 2D Gamma results for film at 5%/3mm in the axial (left) and sagittal (right) planes for Trial 1 of APRL Plan**

The average over all 3 trials for the 2D gamma had 88% pixels pass at 5%/3mm in the axial plane and 93% pass in the sagittal plane. Full results from each trial are listed in the Appendix.

The large volume calibration resulted in a dose response of  $0.0599 \pm 0.003 \Delta\text{OD} \cdot \text{Gy}^{-1} \cdot \text{cm}^{-1}$  and is shown Figure 4-10. The calibration was applied to convert the OD to dose for the PRESAGE<sup>®</sup> and then the dose was normalized to the TLD in the PTV.

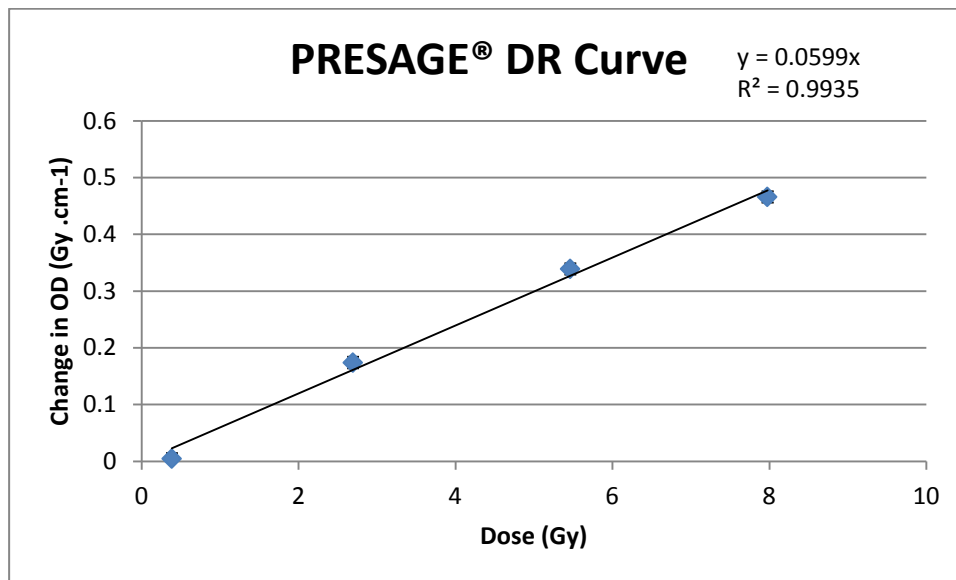


**Figure 4-10: Dose Response for APRL PRESAGE<sup>®</sup> Batch**

The matching line profiles from the imaging insert are shown in Figure 4-11 through Figure 4-13. The largest discrepancy of 4.7% appeared near the edge of the dosimeter. In other locations the doses were within 1%.

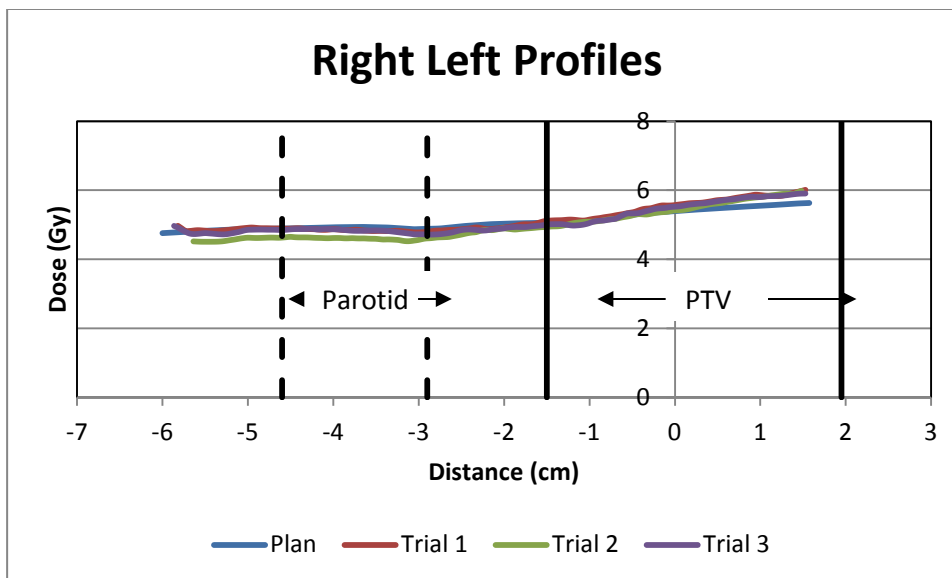


Figure 4-11: PRESAGE<sup>®</sup> Right-Left dose profiles for APRL plan

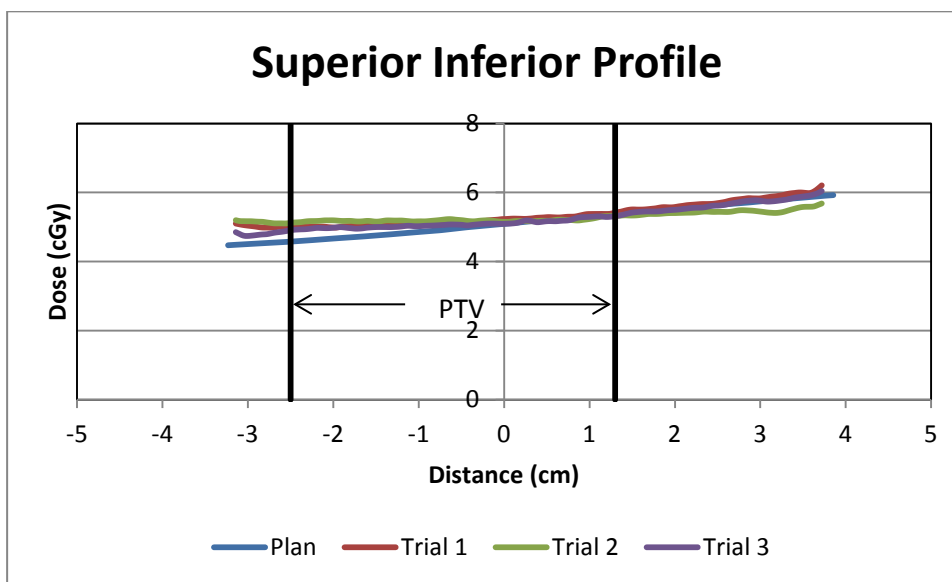


Figure 4-12: PRESAGE<sup>®</sup> Superior Inferior Profiles for APRL plan

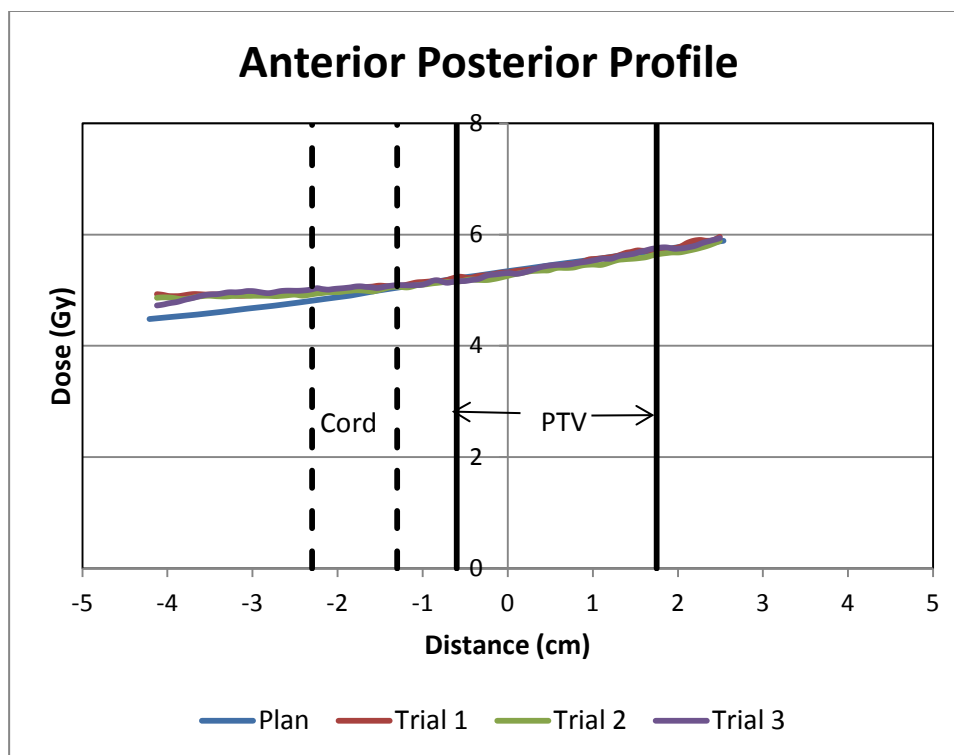


Figure 4-13: PRESAGE<sup>®</sup> Anterior-Posterior profiles for APRL plans

The gamma results measured using 5%/3mm criteria for all three trials are summarized below in Table 4-5. The column labeled PRESAGE<sup>®</sup> contains the 2D gamma results in the planes specified. The last column shows the average for the 3D volume of the PRESAGE<sup>®</sup> minus the 5 mm edge artifact.

Area of Interest	Film	PRESAGE <sup>®</sup>	PRESAGE <sup>®</sup> 3D - 5mm
Axial	88±3.2%	97±0.6%	X
Sagittal	93±1.2%	99±0.9%	X
Coronal	X	99±0.9%	X
Volume	X	X	94±0.7%

Table 4-5: PRESAGE<sup>®</sup> average gamma results at 5%/3mm for APRL plans

The gamma results for the axial film plane (88% pixels passing) were 9% lower than for the axial PRESAGE<sup>®</sup> plane (97% pixels passing) and varied as much as 6.4% across 3 trials. The sagittal and

coronal planes as well as the volumetric gamma results all demonstrated pixel passing rates at or above 93%. The variation of the measurements stayed in a range of  $\pm 1\%$  across all the trials.

#### 4.3.2 IMRT Plan Results

The average TLD results for all 3 trials for the IMRT plan are listed below in Table 4-6.

TLD Location	Measured Dose (cGy)	Predicted Dose (cGy)	Measured/Predicted Dose	COV
Primary PTV Sup Post	668	686	0.97	0.73%
Primary PTV Inf Post	689	688	1.00	1.68%
Primary PTV Sup Ant	682	688	0.99	0.95%
Primary PTV Inf Ant	686	690	0.99	0.98%
Organ at Risk Sup	315	318	0.99	0.72%
Organ at Risk Inf	300	300	1.00	2.52%
Secondary PTV Sup	302	308	0.98	1.48%
Secondary PTV Inf	329	333	0.99	2.33%

Table 4-6: Average TLD Results for IMRT Plan

The ratios of measured TLD results were between 0.97 and 1.00 and remained within the pass rate of 5%. The COV stayed below 3%.

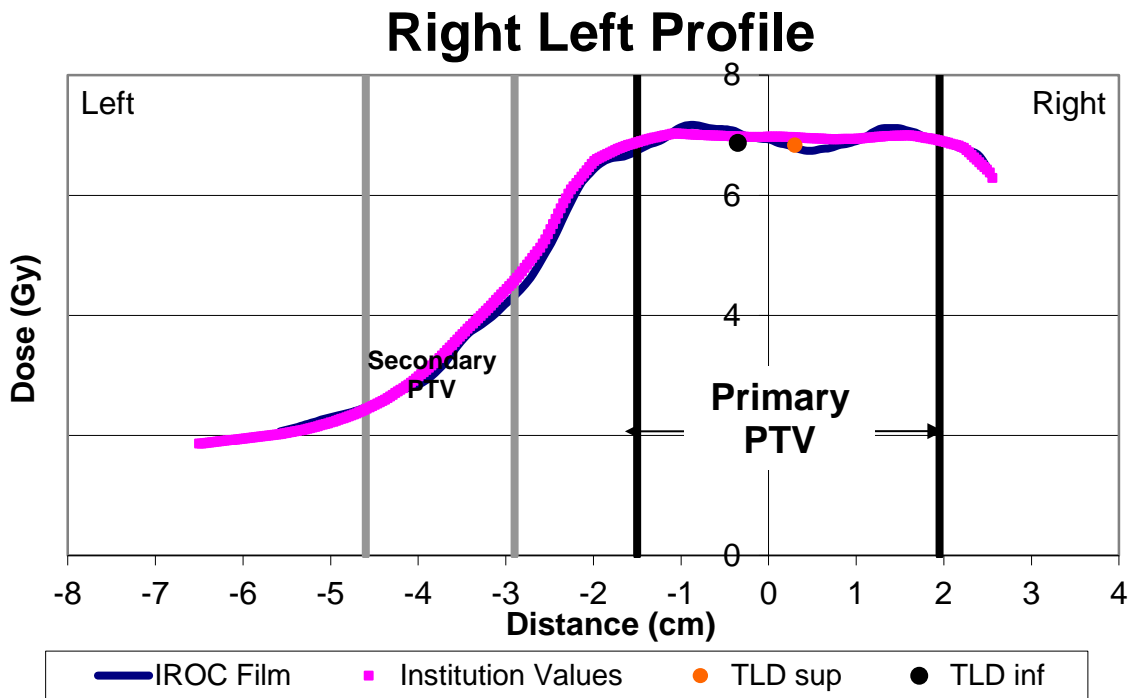


Figure 4-14: Right-Left Film Profiles for Trial 1 of IMRT plan

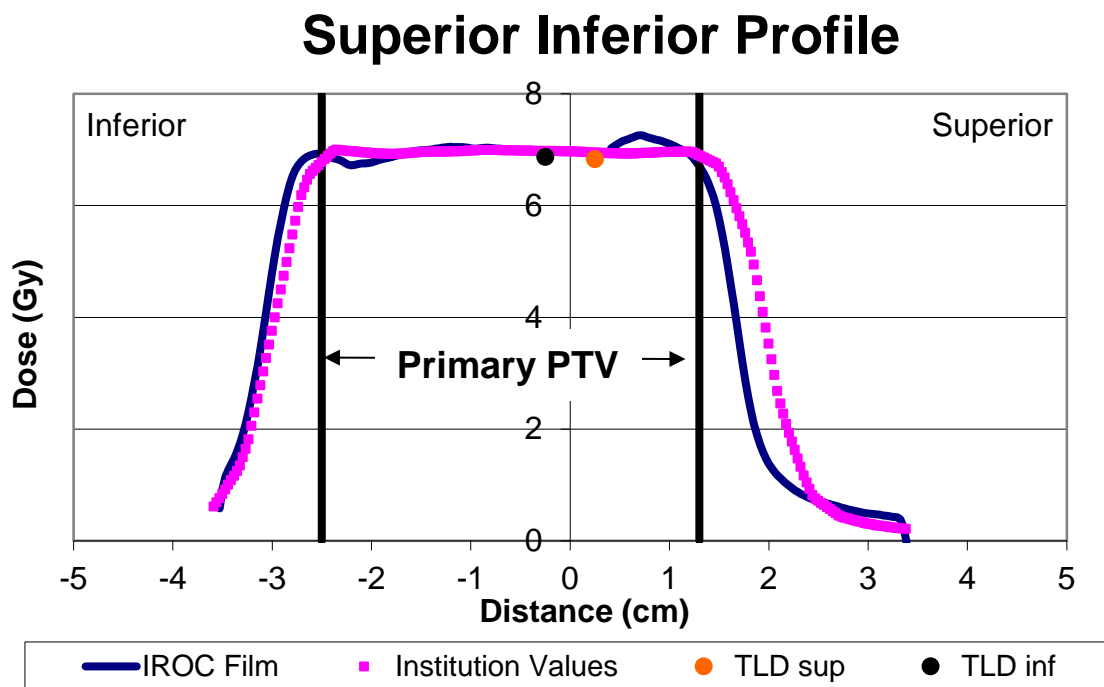


Figure 4-15: Superior-Inferior film profile for Trial 1 of IMRT plan

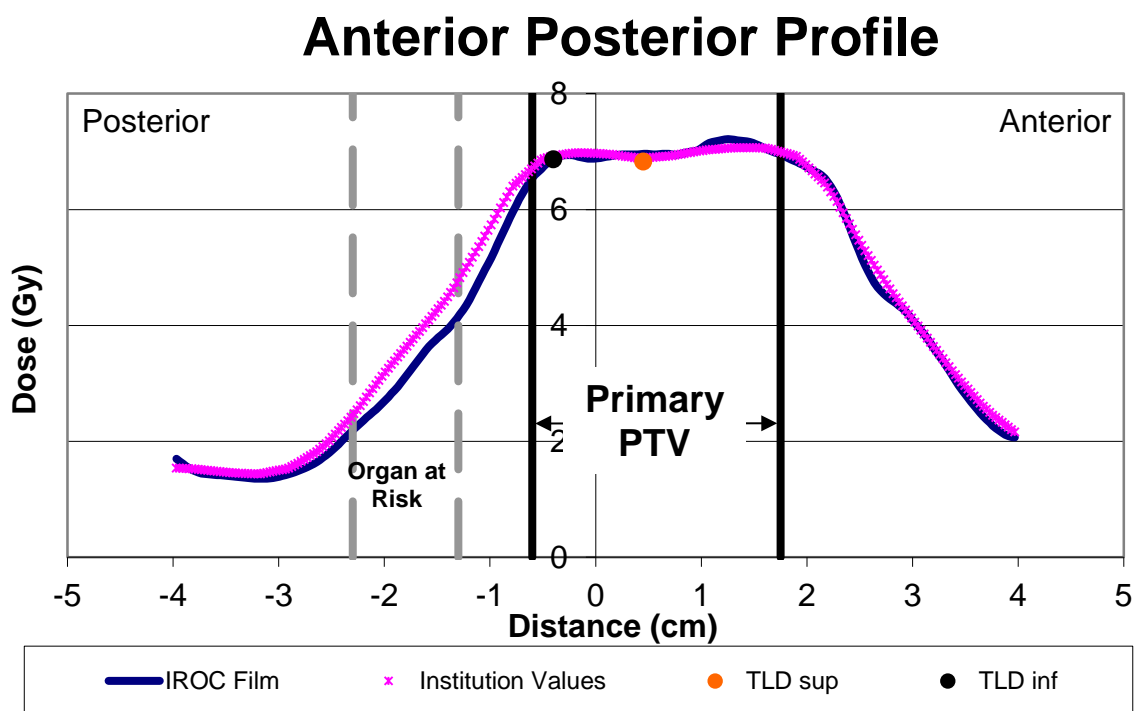
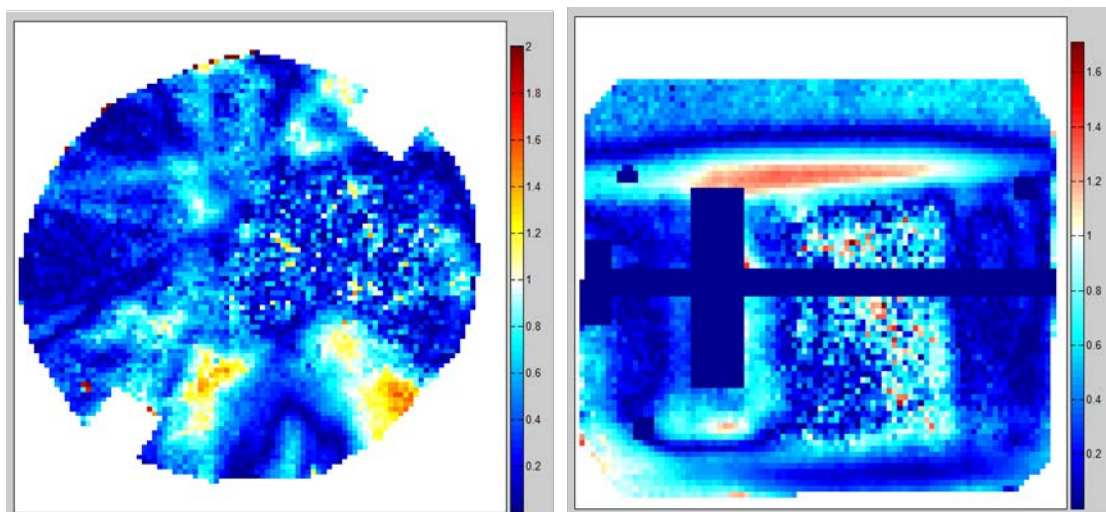


Figure 4-16: Anterior-Posterior film profile for Trial 1 of IMRT plan

Figure 4-14 through Figure 4-16 are the film profiles results for Trial 1. The superior-inferior profile showed a 2 mm difference DTA near the superior edge of the dose plane and the anterior-posterior profile showed a 1 mm difference in DTA through the organ at risk. There was no DTA difference in the right-left profile.



**Figure 4-17: 2D Gamma results for film at 5%/3mm in the axial (left) and sagittal (right) planes for Trial 1 of IMRT plan**

The average 2D gamma had 93% pixels pass using 5%/3mm criteria in the axial plane and 90% pass in the sagittal plane. Full results from each trial are listed in the Appendix.

The large volume PRESAGE<sup>®</sup> dose calibration resulted in a dose response  $0.0292 \pm 0.015$   $\Delta OD \cdot Gy^{-1} \cdot cm^{-1}$  and is shown in Figure 4-18.



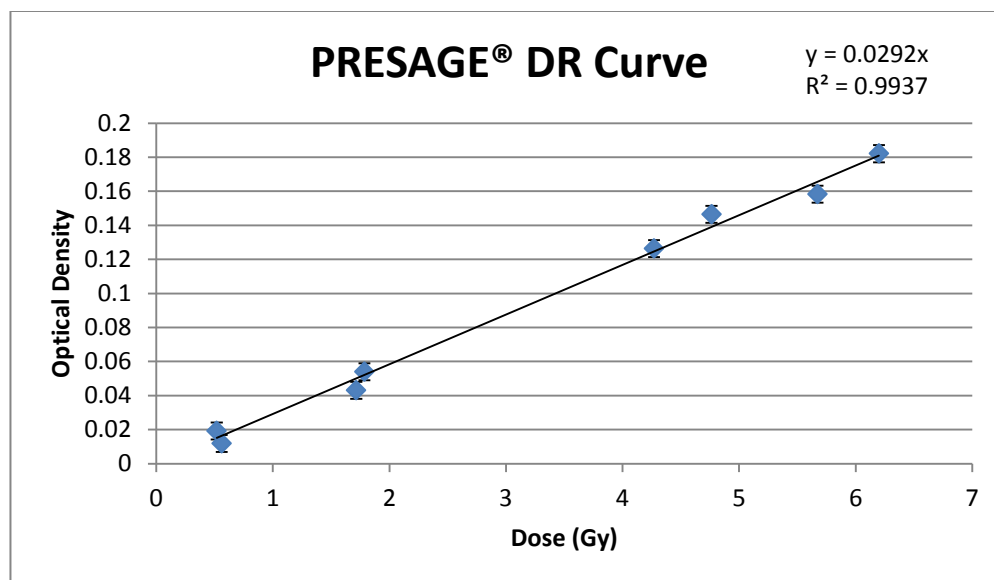


**Figure 4-18: Dose Response Curve for IMRT PRESAGE® Batch**

The dose line profiles for the PRESAGE® dosimeters are shown in Figure 4-19 through Figure 4-21. All 3 trials of PRESAGE® measurements are shown in the graphs. The dose calibration curve was applied and then the dose was normalized to the TLD in the PTV. Good agreement was seen in comparison to the treatment plan which is shown by the blue curve.

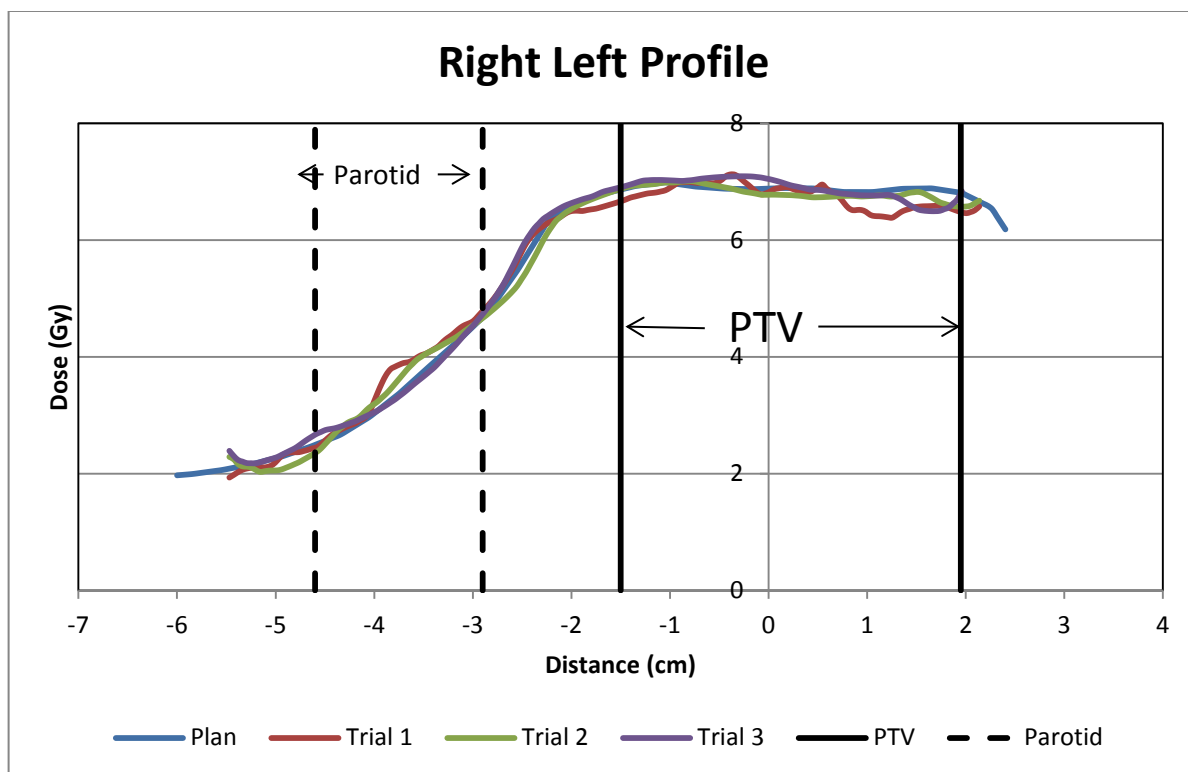


Figure 4-19: Right-Left PRESAGE<sup>®</sup> profiles for IMRT plan

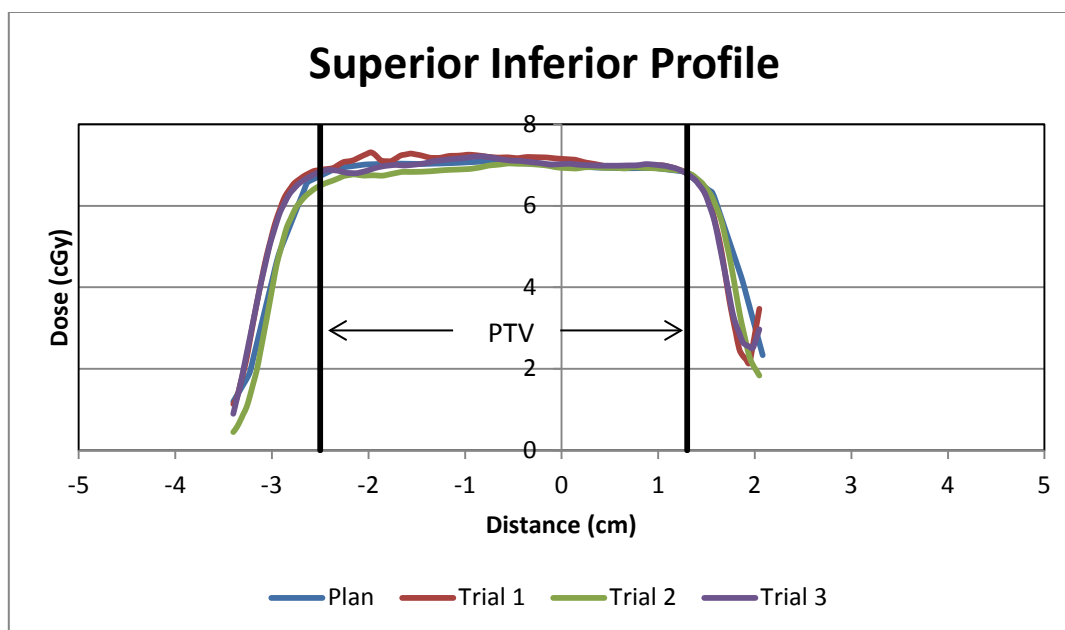


Figure 4-20: Superior-Inferior PRESAGE<sup>®</sup> profiles for IMRT plan

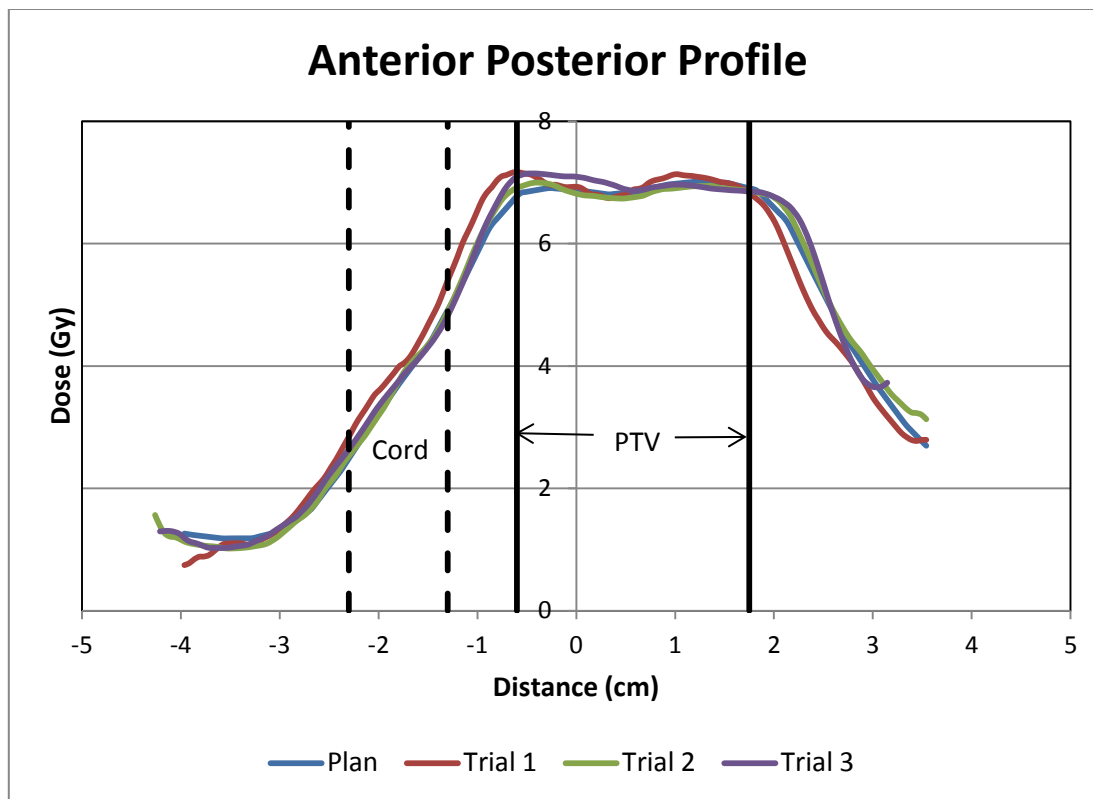


Figure 4-21: Anterior-Posterior PRESAGE<sup>®</sup> profiles for IMRT plan

The gamma results using a 5%/3mm criteria for all three trials are summarized below in Table 4-7.

	Film	PRESAGE <sup>®</sup>	%difference	PRESAGE
		Slice		
Axial	93±1.4%	95±2.6%	2.3%	X
Sagittal	90±2.6%	96±2.0%	6.0%	X
Coronal	X	98±1.1%	X	X
Volume	X	X	X	96±2.0%

Table 4-7: PRESAGE<sup>®</sup> average gamma results at 5%/3mm for the IMRT plan

The column labeled PRESAGE<sup>®</sup> contains the 2D gamma results in the planes specified. The last column shows the average for the 3D volume of the PRESAGE<sup>®</sup> minus the 5 mm edge artifact. The film passes at or above 90% at the criteria of 5%/3mm in both planes. The PRESAGE<sup>®</sup> passing results are higher by 2% in the axial plane and 6% in the sagittal plane with at least 95% pixels passing at 5%/3mm for a 2D slice from the PRESAGE<sup>®</sup> dosimeter. The 3D gamma had 96% pixels passing. Uncertainties are reported to two significant figures based on the precision of data reported by CERR.

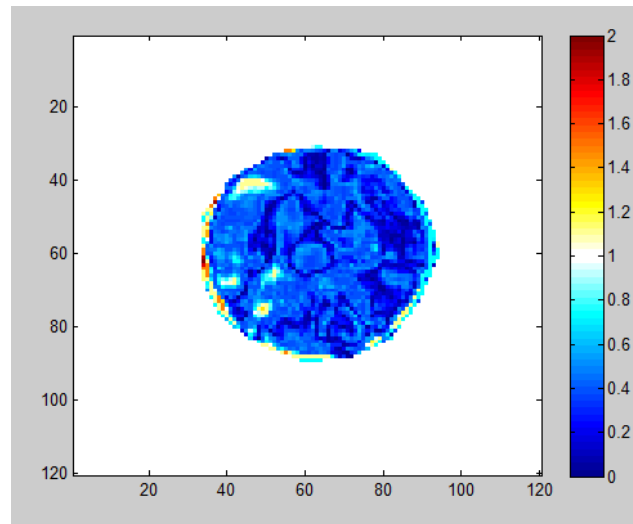


**Figure 4-22: IMRT Trial 1 Gamma Index at 5%/3mm with 96% of pixels passing**

Figure 4-22 is an example of the gamma index map for PRESAGE<sup>®</sup>. The gamma results of the trials had a standard deviation of  $\pm 3\%$  across 3 trials.

#### **4.3.3 Gamma Constraints**

Table 4-7 summarizes the average results over three trials for gamma analysis performed using 3%/3mm, 5%/3mm and 7%/4mm DTA.

		<b>Film</b>	<b>PRESAGE® Slice</b>	<b>PRESAGE® 3D</b>
<b>Axial Total</b>	3%/3mm	85±1.6%	85±2.7%	X
	5%/3mm	93±1.4%	95±2.6%	X
	7%/4mm	99±0.47%	98±1.0%	X
<b>Sagittal Total</b>	3%/3mm	85±1.4%	89±2.3%	X
	5%/3mm	90±2.6%	96±2.0%	X
	7%/4mm	99±0.82%	100±0.0%	X
<b>Coronal Total</b>	3%/3mm	X	94±1.9%	X
	5%/3mm	X	98±1.1%	X
	7%/4mm	X	99±0.84%	X
<b>Total Volume</b>	3%/3mm	X	X	90±2.2%
	5%/3mm	X	X	96±2.0%
	7%/4mm	X	X	100±0.24%
<b>PTV Total</b>	3%/3mm	X	X	96±0.93%
	5%/3mm	X	X	100±0.058%
	7%/4mm	X	X	100±0.0%
<b>Parotid Total</b>	3%/3mm	X	X	94±4.7%
	5%/3mm	X	X	99±2.2%
	7%/4mm	X	X	100±0.0%
<b>Cord Total</b>	3%/3mm	X	X	92±8.1%
	5%/3mm	X	X	98±2.3%
	7%/4mm	X	X	100±0.0%
<b>Normal Tissue Total</b>	3%/3mm	X	X	90±2.4%
	5%/3mm	X	X	96±1.0%
	7%/4mm	X	X	100±0.27%

**Table 4-8: Pass rates for 3 levels of gamma constraints**

The structures contoured within the PRESAGE® dosimeter were also calculated as they are available to view once the 3D gamma has been calculated. The more generous constraint of 7%/4mm proved too lax for evaluation. The results were at or near 100% for all dose measurements. All PRESAGE® measurements passed the 3%/3mm gamma constraint with a passing rate above 85%. The passing rates at the 5%/3mm constraint are as shown in Table 4-7 and demonstrated passing rates above 95%. The total volume 3D gamma and the normal tissue 3D gamma (comprised of the total volume minus all contoured structures) had pixel passing rates of 90% for 3%/3mm, 95% for 5%/3mm and 100% for 7%/4mm. The individual structures had higher pass rates with the lowest result being the

parotid which showed 92% of pixels passing at 3/3mm. At 5%/3mm the individual structures (PTV, parotid and cord) were at or above 98% pixels passing.

## 4.4 Discussion

### 4.4.1 Open Field Plan

The simplified scenario of the APRL was created as an end-to-end test of phantom irradiations before performing more complex irradiations. This was the first irradiation utilizing a TPS to design an irradiation for a PRESAGE<sup>®</sup> dosimeter in this study and the first data to compare measured to calculated dose distributions. The TLD data showed the dose delivery in the major structures was correct and the dose line profiles were also acceptable. The PRESAGE<sup>®</sup> dose line profiles showed an increase in dose near the edge of the field close to 5%. These line profiles were replicating the film profiles and neared the optical edge artifact of the PRESAGE<sup>®</sup>. It was decided for future analysis to avoid the optical artifacts that would perturb the dose field.

It was not expected for PRESAGE<sup>®</sup> to have a passing percentage which was 6 -10 % different. One reason for this might be the thickness of the film itself. The film thickness is 0.28 mm (24). The PRESAGE<sup>®</sup> 2D gamma does take the gamma calculation over the 1 mm thick slice. This extra dimension can increase the probability of finding a passing pixel within the gamma constraints as shown by Pulliam *et. al.* (27).

Another issue discovered was with the film/TLD insert. The current film is thicker than when the phantom insert was originally designed. Pressure marks on the film from being inserted and removed from the phantom caused aberrations in dose readout. More care was taken after this study in cutting film and handling cut-film to minimize any other markings.

The PRESAGE<sup>®</sup> irradiations show one major condition for which the user should be aware of: lack of registration. Looking at the dose profiles one can see this. Registration based on fiducials that were available in x-ray CT and optical CT was not successful. Physical fiducials that could be viewed in x-ray CT distorted optical-CT imaging. Holes were drilled in the top of a PRESAGE<sup>®</sup>

dosimeter to show an air gap in the x-ray CT did not penetrate the top edge artifact of the dosimeter and could not be identified in the optical readout. Deeper holes were avoided because of concern that they would interfere with contoured dose volumes. The PRESAGE<sup>®</sup> registration to the TPS had to be done qualitatively. This lessened the reproducibility. A registration system that fits within phantoms (current BBs do not) is needed to increase precision. Another option would be to coordinate the optical system and CERR to automatically align coordinates using the registration base attached to PRESAGE<sup>®</sup> for optical scanning alignment. The current HN phantom was not designed with depressions for interlocking with the optical alignment base. Overall, the PRESAGE<sup>®</sup> irradiation and analysis was within the gamma passing criteria and considered to be of potential use.

#### **4.4.2 IMRT Plan**

A clinically relevant IMRT plan was used to irradiate the HN phantom. The film and TLD results agreed with the TPS IMRT dose calculation showing a correctly irradiated phantom. Currently, the passing criteria at IROC-Houston for this phantom is 85% pixels passing at 7%/4mm. The film passes at or above 90% at the stricter criteria of 5%/3mm in both planes. The PRESAGE<sup>®</sup> passing results are higher with at least 95% pixels passing at 5%/3mm for a 2D slice from the PRESAGE<sup>®</sup> dosimeter. This confirms first part of the hypothesis which states the PRESAGE<sup>®</sup> 3D dosimeter will agree with 2D measurements to within  $\pm 5\%/3\text{mm}$  using a gamma index analysis. The PRESAGE<sup>®</sup> dosimeter performed at least as well as the “gold-standard” (for this study) film/TLD system. The increase in passing pixels was comparable to the results seen with the APRL irradiation.

#### **4.4.3 Gamma Constraints**

Gamma constraints have been used for 2D dose measurements since Low *et al.* introduced the methodology in 1998 (26). While TG 119 has recommended gamma constraints to be used for IMRT evaluation it was truly intended for planar dose distribution (49). One study by Pulliam *et al* used Monte Carlo calculations and found an increase in passing pixels of up to 2.9% when comparing 3D and 2D gamma analysis (27). In 2014, this was the first study to closely look into the

difference in gamma results between planar and volumetric dose distributions. To our knowledge this study is the first compare planar and volumetric dose measurements for gamma analysis comparison. Theoretically the third dimension should increase the percentage of passing voxels but it is unknown by what percentage.

The PRESAGE<sup>®</sup> dosimeters have consistently shown a higher pass rate compared to the film data in the previous work using 5%/3mm as a constraint. Two constraints other than 5%/3mm were chosen for evaluation for this study: the commonly used 3%/3mm criteria and the passing criteria used by IROC of 7%/4mm. The more generous constraint of 7%/4mm proved too lax for evaluation. The results were near or at 100% for all dose measurements. The 3%/3mm gamma constraint passed all volumetric calculations with a passing rate above 87%. The standard deviation of the volumetric PRESAGE<sup>®</sup> measurements also increased at the tighter constraint. This might be attributed to a slight registration misalignment being caught in 3D. A minor rotation in registration might not be detected in planar analysis but the structure volume misalignment between trials could be magnified.

With the increase in error for volumetric data at the tighter constraint, we decided to continue working with the 5%/3mm gamma constraint. To account for the deviations over the measured data and the intention to use this phantom in the IROC phantom program, we chose passing cutoffs of 85% passing pixels at a gamma constraint of 5%/3mm to be considered passing in planar QA while 90% passing pixels at 5%/3mm to be passing volumetric QA. The tighter constraint or a higher passing percentage (or both) could be used in the future if the standard deviation of PRESAGE<sup>®</sup> measurements decreased and more irradiation continue to show reproducibly high passing percentages.. Improvement in registration could allow the more common 3%/3mm constraint to be used with this HN phantom and the PRESAGE<sup>®</sup> dosimeter.



## Chapter 5 – Specific Aim 4

### 5.1 Rationale

The 3D PRESAGE<sup>®</sup> QA system had been verified against the commissioned film/TLD system in the previous work of this study. Any new dosimetry system should not be implemented unless it improves current outcomes. The phantom program at IROC-Houston is well defined and including PRESAGE<sup>®</sup> would only be advised if a quantifiable advantage was obtained. The disadvantages of a longer evaluation time and increase in cost only left the potential benefits of a measured 3D data set as a benefit that warrants inclusion of the PRESAGE<sup>®</sup> dosimeter into the phantom program. The aim of this section was to test the second part of the hypothesis to evaluate whether 3D dataset could detect errors missed by the current 2D system. And if the volumetric measurement did detect an error, then how much of a clinical impact would this error have on the treatment delivery? To test this part of the hypothesis the IMRT plan was modified to introduce different errors into the plan. These modified plans were then compared to the previously measured dataset using a gamma index analysis. Secondly, since PRESAGE<sup>®</sup> yields volumetric data, the NTCP for the parotid gland was calculated using the measured dose and the calculated dose from each modified treatment plan. A 5% change in NTCP between calculated and measured dose data was considered clinically significant. This specific aim was completed in 2 parts performed simultaneously:

- Modify the IMRT plan to create errors and test with 2D and 3D gamma index analysis and identify situations where a plan passes a 2D quality assurance but fails with the 3D measurement.
- Calculate the NTCP for the parotid gland over the original measurement and the modified plans. Identify which plans that only failed the 3D gamma index differed by 5% of the expected NTCP.

## 5.2 Methods

The original IMRT plan was modified several times to test whether a 3D measurement would catch errors where the 2D measurement did not. For cost effectiveness, i.e. minimize the number of PRESAGE<sup>®</sup> dosimeters to be manufactured and irradiated, the measured dose distribution from PRESAGE<sup>®</sup> irradiated using the original plan was compared to changes made in the TPS. This was done with confidence because previous work had shown the dosimeter to correctly measure the calculated dose distribution.

Eight modified plans were used to recalculate the gamma index. Each plan was intended to showcase a scenario that might pass 2D quality assurance while failing a true 3D measurement. The first modification was a change in the dose calculation engine. During clinical treatment planning the Adaptive Convolve engine is used to calculate dose for plans to be reviewed. Because it does a coarser calculation in regions where TERMA (Total Energy Released in Matter) is relatively constant, it is quicker than the Collapsed Cone Convolution (CC Convolution) but also less accurate.. Final dose calculation was calculated using CC Convolution. The modified plan “Adaptive Convolve” illustrated the situation when the final dose calculation was not changed to CC Convolution.

The second and third modified plans changed the dose grid used for calculation. Chung *et al* studied the effect varying the dose calculation grid had on dose in head and neck IMRT (50). The calculation dose grid used for this study was 3 mm as used in our clinic. The “2 mm Dose Grid” plan reduced the dose calculation grid down to a size that is not used for HN treatments at the time of the experiment. The “4 mm Dose Grid” plan increased the dose grid beyond the accepted 3 mm for this treatment site.

The fourth modification simulated importing the wrong patient plan to the treatment machine. “Extended Parotid” plan increased the size of the parotid 4 mm in the inferior direction and out of

the primary beam. This was a small change to increase the volume of a structure used for calculation in the inverse planning.

The fifth modification involved creating a cold spot near the PTV that was not caught by a chart check. A structure was placed near the PTV as an avoidance structure to help in the planning process and was supposed to be removed for the final treatment calculation. In this scenario, the plan trial with the avoidance in place was accidentally used as the final plan and exported for treatment.

The sixth modification titled “Re-Optimization” was an example of a plan being re-optimized in inverse planning after the plan had been exported for gamma index analysis. This led to a different optimization (with the exact same constraints) for the actual plan delivery versus the dose calculation used to compare to the measured dose.

The last three modifications are examples of delivery errors. The first delivery error simulated a gantry offset. “Angle 122” moved the gantry 2 degrees from the intended beam angle of 120. The other two delivery errors involved a malfunctioning Multi-Leaf Collimator (MLC). MLC errors are not always detected during IMRT QA and even less so when testing with doing QA with a composite plan (51). A 3D measurement might have an increased sensitivity to MLC errors. Two plans were created to simulate MLC error commonly regarded as a sticky leaf. “Sticky Leaves 1” and “Sticky Leaves 2” closed 2 to 3 leaves from the MLC for beam angle 80 and 40 respectively.

The NTCP was calculated for all three trials of PRESAGE<sup>®</sup> irradiations and compared to the treatment plan’s calculations. The dose in CERR was increased to cover a full treatment and the NTCP function in CERR and the inputs from Dijkema *et al* of  $n=1$ ,  $TD50 = 40.5$  and  $m=0.36$  were input into the program (48). The dosimeter with the smallest difference between plan and measurement for NTCP was used to compare to all further plan modifications.

Each modified plan’s dose was imported into CERR and the dose was scaled to cover a full treatment. The NTCP was calculated for each plan. Gamma index analyses in 2D and 3D were also performed at a gamma index of 5%/3mm with 85% pixels passing considered passing 2D quality

assurance and 90% pixels passing considered passing 3D quality assurance. Plans that passed 2D quality assurance but failed 3D quality assurance were sorted by the percent change in NTCP. A 5% change was considered clinically relevant.

### 5.3 Results

The first step was to determine the best PRESAGE<sup>®</sup> dosimeter for analysis. Table 5-1 shows the results of the NTCP change from the original IMRT plan and each trial. Trial 3 had the smallest change in percent from the original at 0.64% and was used for all gamma analysis and has the baseline for the change in NTCP with the modified plans. Figure 5-1 shows the GUI used in CERR to model NTCP for Trial 3.

Dose name	NTCP %	change in %
<b>Original IMRT Plan</b>	25.4%	0.00%
<b>Trial 1 Measurement</b>	29.4%	4.06%
<b>Trial 2 Measurement</b>	26.7%	1.37%
<b>Trial 3 Measurement</b>	26.0%	0.64%

Table 5-1: NTCP values from Measured Dose

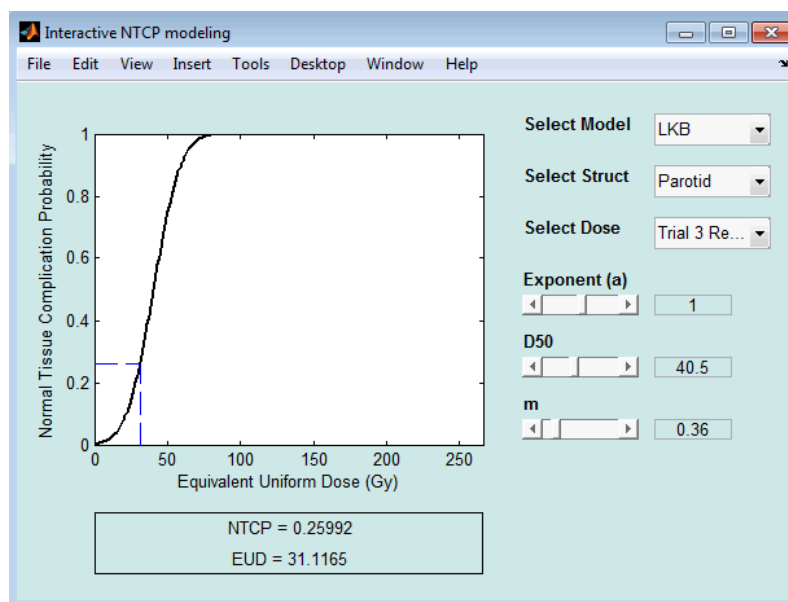


Figure 5-1: NTCP modeling from CERR for Trial 3 dose measurement

Each modified treatment plan was imported to CERR and analyzed using a 5%/3mm gamma constraint identified in the previous section. The percentages of passing pixels for each plan are summarized in Table 5-2. Furthermore the NTCP was modeled for each plan. Table 5-3 summarizes the NTCP results.

For the change in dose algorithm to Adaptive Convolution from CC Convolution, the 2D gamma index analysis showed 96% pixels passing for 5%/mm criteria in both the axial and sagittal planes. The 3D gamma had a lower passing percentage of 91% pixels passing for 5%/3mm criteria. This plan passed both QA tests. The NTCP over the parotid gland increased by 2.4% from the original measurement.

The 2 mm dose grid test passed with at least 96% pixels passing in both planes for 2D analysis using 5%/3mm criteria. The 3D gamma analysis showed 92% of pixels passing using 5%/3mm. The NTCP increased by 3.84% from the measured probability. The 4 mm dose grid plan passed 2D QA with at least 90% of pixels passing using 5%/3mm for both planes. The 3D QA failed with 89% pixels passing at 5%/3mm. The passing cutoff was 90% pixels passing. The NTCP increased 4.85%. The extended parotid plan passed 2D QA with at least 86% of pixels passing for both planes. The plan failed 3D QA with only 82% of pixels passing using 5%/3mm criteria. The NTCP decreased 9.23%.

The plan that left a cold spot within the PTV failed QA in both 2D and 3D with the 5%/3mm gamma criteria. Only 63% of pixels passed in the axial plane and 81% of pixels passed in the sagittal plane. 66% of pixels passed in the 3D volume. The NTCP increased 2.38%.

The Re-Optimization plan failed 2D QA with only 75% pixels passing the sagittal plane for 5%/3mm criteria. The plan also failed in the 3D QA with 79% pixels passing using 5%/3mm. The NTCP increased by 5.61%.

The beam angle plan passed 2D gamma analysis with at least 93% of pixels passing at 5%/3mm in both planes. The 3D gamma analysis showed 93% of pixels passing for 5%/3mm. The NTCP increased by 0.97%. Both sticky leaves plan 1 and 2 passed QA with 2D gamma constraints having at least 96% pixels passing for plan 1 and 94% pixels passing for plan 2 at 5%/3mm. The 3D gamma had a passing rate of 91% and 90% at 5%/3mm for plans 1 and 2 respectively. The NTCP increased by 4.2% for plan 1 and by 2.99% for plan 2.

	Adaptive Convolve	Extended Parotid	2mm Dose Grid	4mm Dose grid	Re-Optimization	Cold Spot	Beam Angle 122	Sticky Leaves	Sticky Leaves 2
<b>Axial Slice</b>	96%	86%	97%	96%	85%	63%	96%	96%	94%
<b>Sagittal Slice</b>	96%	94%	96%	90%	75%	81%	93%	97%	98%
<b>3D Gamma</b>	91%	82%	92%	89%	79%	66%	93%	91%	90%

Table 5-2: 2D and 3D Gamma Results at 5%/3mm

Dose description	Pass 2D?	Pass 3D?	NTCP %	change in %
Adaptive Convolve	yes	yes	28.4%	2.4%
2mm dose grid	yes	yes	29.8%	3.8%
<b>4 mm dose grid</b>	<b>yes</b>	<b>no</b>	<b>30.8%</b>	<b>4.9%</b>
<b>Extended Parotid</b>	<b>yes</b>	<b>no</b>	<b>16.8%</b>	<b>9.2%</b>
Re-Optimization	no	no	31.6%	5.6%
Cold Spot	no	no	28.4%	2.4%
Beam Angle 122	yes	yes	27.0%	1.0%
Sticky Leaves	yes	yes	30.2%	4.2%
Sticky Leaves 2	yes	yes	29.0%	3.0%

Table 5-3: Gamma Index and NTCP results. Highlighted results passed a 2D evaluation and failed a 3D evaluation.

Only 2 plans passed a 2D gamma criterion and failed the 3D gamma criterion. Of those two, only the “extended parotid” plan showed a change in NTCP of 5%. The plan changing the

calculation dose grid to 4mm from 3mm was close with a NTCP change of 4.9%. There were no instances where the 3D gamma evaluation passed a plan the 2D evaluation failed.

The second part of the hypothesis stated the PRESAGE<sup>®</sup> dosimeter will detect dose distribution discrepancies for complex treatments not detected by 2D planar film measurements that will result in a 5% difference in NTCP. In fact, of nine experiments, the PRESAGE<sup>®</sup> dosimeter detected a discrepancy resulting in more than 5% difference in NTCP that was not detected by 2D planar measurements. Consequently, while the hypothesis is not conclusively demonstrated, these results argue that the hypothesis cannot be rejected.

## 5.4 Discussion

The last section of this study evaluated different treatment scenarios and how a PRESAGE<sup>®</sup> volumetric dose measurement affected outcome compared to 2D evaluation. Seven of the modified plans passed 2D quality assurance at 5%/3mm. This result was surprising as many institutions using the IROC phantom are unable to pass at a higher pass criterion. This phantom has shown its ability to catch treatment planning as well as delivery errors. The PRESAGE<sup>®</sup> dosimeter and film analysis was shown as comparable in Table 4-7 and we did not expect the PRESAGE<sup>®</sup> to pass this amount of modified plans.

Both plans that altered the MLC (Sticky Leaves and Sticky Leaves 2) passed 2D and 3D. The 3D gamma had a lower pass rate for both plans by at least 4-5%. We expected a 3D gamma to have an equal or higher pass rate for a truly passing irradiation. The lower pass rate from the 3D gamma showed the MLC modification does have a greater dose discrepancy over the volume than can be measured with planar QA suggesting the 3D measurement has an increased sensitivity. The adaptive convolve plan also had a lower 3D passing rate when compared to the 2D. This dose algorithm change was another subtle error that showed a greater impact when a full volumetric dose was studied. If PRESAGE<sup>®</sup> was brought into a QA system more routinely, this low of a score might flag further evaluation.

The plans that failed all quality assurance were the re-optimization plan and the intentional cold spot plan. Both plans involved inverse planning (instead of a single dose re-calculation without optimization) and did not change the dose field significantly enough to be detected. These results were not surprising. To detect a change, a significant number of voxels need to experience dose adjustments and the Adaptive Convolve and CC Convolution use the same dose algorithm but calculate on a different grid in parts of the plan.

The two plans that only failed using a 3D gamma analysis were the extended parotid plan and the 4 mm dose grid. The extended parotid plan was expected to fail as it changed the dose field outside of the planes used for 2D analysis. With a measured volumetric dose on hand a dose volume histogram (DVH) was easily created to look at any dose discrepancies in the major structures.

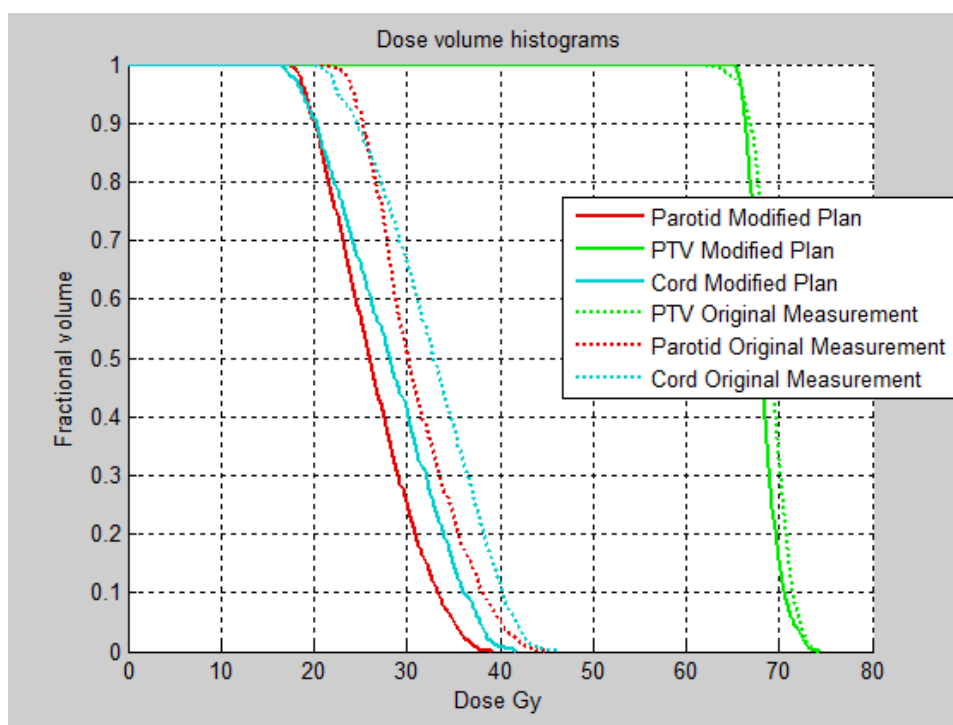


**Figure 5-2: Dose Volume Histogram for the Extended Parotid plan and Trial 3 measurement**

Figure 5-2 shows the DVH for the extended parotid plan. The modified dose to the cord and the parotid gland were lower across the volume than the original plan measurement. A true measured DVH can be made for any measurement taken with the PRESAGE<sup>®</sup> dosimeter. While impractical to



look at every parameter of data that PRESAGE<sup>®</sup> measured it is invaluable to have the information when troubleshooting a low-scoring or failing irradiation.

The 4mm dose grid plan also failed with the 3D gamma. This dose grid is larger than the 3 mm dose calculation grid typically used at our institution for head and neck patients. Niemierko *et al* noted that the larger the dose penumbra, the greater the interpolation errors are for a given grid size (52). Yan *et al* recommended no larger than a 2mm dose grid size for HN cases for this same reason even though 3 mm and 4 mm dose grid sizes were suitable for most cases of IMRT (51). It is considered for this plan the interpolation errors over volume caused the failure in 3D.

NTCP is a metric that can be used to predict clinical outcome in patients. This is a volumetric calculation and easily calculated in CERR with our volumetric dataset. With all of the plan modifications, only 2 plans had a 5% change in NTCP: Re-Optimization and Extended Parotid. The Re-Optimization plan failed planar QA and would not have been used for treatment but the Extended Parotid case only failed using 3D gamma analysis. The NTCP change of 9.2% suggests a change in clinical outcome could be possible when treating with this modified plan. This showed PRESAGE<sup>®</sup> was able to catch an error that could have an impact where the original film/TLD insert did not. The second plan to only fail when tested with a 3D gamma had a change of NTCP of 4.9%. While not at the 5% level for the hypothesis of this project this number could still be considered significant to come clinicians. Further investigation into biological metrics with 3D measured datasets should be conducted to quantify the impact a true measured 3D dataset could have for a clinic.

With 3D measurements, once a gamma analysis had failed the full volumetric dose measurement was already in place to further investigate the problem without a re-irradiation. This can be a time and cost saving technique to identify the cause of the discrepancy. In this case, by looking at the 3D gamma difference and the DVH a physicist could suggest an institution needs to confirm they treated with or uploaded the correct treatment plan for analysis prior to suggesting a re-irradiation with the same plan. Being able to investigate with the failing dose measurement instead of

having to re-irradiate and hope to re-create the error can help increase quality control for patient-specific IMRT QA.

## Chapter 6 – Conclusion

### 6.1 Summary

This project was intended to test whether a measured 3D dataset could provide greater value than the current process that could affect the quality of care of patients in the future. This project was done using a PRESAGE<sup>®</sup> dosimeter in an IROC-Houston HN phantom. We hypothesized that complex dose distributions measured with the PRESAGE<sup>®</sup> 3D dosimeter will agree with 2D measurements to within  $\pm 5\%/3\text{mm}$  using a gamma index analysis. Also, the PRESAGE<sup>®</sup> dosimeter would be able to detect dose distribution discrepancies for complex treatments not detected by 2D planar film measurements that would result in a 5% difference in NTCP.

This project was completed in 4 parts. In the first part an optical-CT system was set up and verified for use. A standard of practice was created to ensure that data measured would be independent of the user. A quality assurance program was designed to verify the optical density measured would be consistent prior to data acquisition. This section created a stable optical-CT scanning protocol for reproducibility and reliability.

The second part of this study assessed the capability of the PRESAGE<sup>®</sup> dosimeters for remote quality assurance. A dose calibration procedure was devised for each bath of dosimeters. The temporal and thermal stability of a 500g dosimeter was studied. We found in this section remote dosimetry was feasible. A dosimeter's thermal and temporal history were important to record and all irradiations need to be performed at room temperature. It was recommended while using PRESAGE<sup>®</sup> as a relative dosimeter, a calibration could be done with cuvettes from the same dosimeter batch.

The third part of the study used the HN phantom from the IROC-Houston phantom program to measure dose distributions from a calculated treatment plan. A gamma index analysis was used to record the percentage of passing pixels for two dosimetry systems: the film/TLD insert credentialed by IROC-Houston and the PRESAGE<sup>®</sup> insert. Various gamma constraints were used for analysis to

attempt to define an appropriate constraint for an acceptable IMRT quality assurance. That data suggest that volumetric dosimetry may be able to use tighter constraints than 2D analysis, but the study of site-by-site investigation of that was not in the scope of this research.

The last section of this project tested whether PRESAGE<sup>®</sup> measurements would be able to detect errors in dose delivery that 2D measurements did not. Furthermore, we wanted to know if these plans that only failed using 3D detection would have a change in the NTCP metric. Treatment plans were modified to create errors. These plans were analyzed using the correctly irradiated PRESAGE<sup>®</sup> dataset from the previous section. Two of the treatment plans passed the 2D gamma index analysis and failed the 3D gamma analysis. One of these plans resulted in a 5% change in NTCP.

## 6.2 Conclusion

Using a 3D dosimeter and optical-CT readout brought new challenges. With a goal of using PRESAGE<sup>®</sup> in the IROC-Houston phantom project, creating a stable readout procedure was necessary. Any discrepancies in the measured dataset needed to be due to dose delivery errors and not from a dosimeter or read-out malfunction. Quality control of the optical-CT scanner and correct handling of the PRESAGE<sup>®</sup> dosimeters allowed us to move forward to using the PRESAGE<sup>®</sup> dosimeter for phantom irradiations.

From the measured dose distributions we concluded the PRESAGE<sup>®</sup> dosimeter did agree with 2D measurements to within  $\pm 5\%/3\text{mm}$  and proved the first half of the hypothesis correct. Various gamma constraints were investigated to try and define a cutoff for passing a gamma index analysis in 3D. As this work continues, more irradiations using different treatment sites would better define the appropriate criteria for a volumetric dataset. The NTCP metric was used to predict a change in patient outcome using 3D dose measurements. One modified treatment plan passed a 2D analysis and failed the 3D analysis with a 5% change in NTCP showing it is possible for the second half of

the hypothesis to be correct. This suggested the volumetric dose measurement could have an impact on clinical outcome.

### **6.3 Future Works**

Volumetric dosimetry is fast changing in these times. Over the course of this project, the scanner, the code used for analysis and the dosimeter itself underwent upgrades. This project outlined a successful procedure for scanning and scanner quality assurance. New formulations of PRESAGE<sup>®</sup> should undergo the same thermal and temporal studies as shown in this project prior to being used for any remote dosimetry. Software upgrades must always be validated prior to use. CERR is an open-source platform that is constantly being changed. Careful consideration is needed before upgrading any of the code.

The most pressing work to be completed for this system is a registration system for the dosimeter with a treatment plan. This would reduce analysis errors and decrease the time it takes a user to measure data. In a full scan and analysis, at this time dose registration with a treatment plan almost always takes the most amount of time to perform correctly. A registration system would also allow for phantom setup errors to be detected. By aligning the measured dose with the planned dose distribution the phantom no longer measures setup error.

This project focused on the HN phantom. More patient sites should be similarly evaluated. This would test the different shapes that PRESAGE<sup>®</sup> could be successfully used in optical-CT and increase the overall dataset for gamma analysis working towards an improved recommendation for gamma analysis constraints with measured volumetric data.

## Appendix

The individual trials are listed below for each dosimeter.

<b>TLD Location</b>	<b>Measured Dose (cGy)</b>	<b>Predicted Dose (cGy)</b>	<b>Measured/Predicted Dose</b>
PTV Sup Post	531	528	1.00
PTV Inf Post	520	519	1.00
PTV Sup Ant	520	526	0.99
PTV Inf Ant	529	521	1.02
Cord Superior	492	486	1.01
Cord Inferior	484	479	1.01
Parotid Superior	500	495	1.01
Parotid Inferior	490	490	1.00

**Table 7-1: TLD Results for Trial 1 from APRL Plan**

<b>TLD Location</b>	<b>Measured Dose (cGy)</b>	<b>Predicted Dose (cGy)</b>	<b>Measured/Predicted Dose</b>
PTV Sup Post	533	528	1.01
PTV Inf Post	535	519	1.03
PTV Sup Ant	536	526	1.02
PTV Inf Ant	533	521	1.02
Cord Superior	498	486	1.03
Cord Inferior	497	479	1.04
Parotid Superior	496	495	1.00
Parotid Inferior	500	490	1.02

**Table 7-2: TLD Results for Trial 2 from APRL Plan**

<b>TLD Location</b>	<b>Measured Dose (cGy)</b>	<b>Predicted Dose (cGy)</b>	<b>Measured/Predicted Dose</b>
PTV Sup Post	526	528	0.99
PTV Inf Post	533	519	1.03
PTV Sup Ant	533	526	1.01
PTV Inf Ant	536	521	1.03
Cord Superior	497	486	1.02
Cord Inferior	494	479	1.03
Parotid Superior	496	495	1.00
Parotid Inferior	499	490	1.02

**Table 7-3: TLD Results for Trial 2 from APRL Plan**

<b>Area of Interest</b>	<b>Film</b>	<b>PRESAGE®</b>	<b>PRESAGE® 3D - 5mm</b>
<b>Axial</b>	87%	98%	X
<b>Sagittal</b>	92%	100%	X
<b>Coronal</b>	X	100%	X
<b>Volume</b>	X	X	94%

**Table 7-4: 2D Gamma Results at 5%/3mm for Trial 1 from APRL Plan**

<b>Area of Interest</b>	<b>Film</b>	<b>PRESAGE®</b>	<b>PRESAGE® 3D - 5mm</b>
<b>Axial</b>	92%	99%	X
<b>Sagittal</b>	94%	98%	X
<b>Coronal</b>	X	99%	X
<b>Volume</b>	X	X	95%

**Table 7-5: 2D Gamma Results at 5%/3mm for Trial 2 from APRL Plan**

Area of Interest	Film	PRESAGE®	PRESAGE® 3D - 5mm
Axial	86%	96%	X
Sagittal	94%	99%	X
Coronal	X	98%	X
Volume	X	X	94%

Table 7-6: 2D Gamma Results at 5%/3mm for Trial 3 from APRL Plan

TLD Location	Measured Dose (cGy)	Predicted Dose (cGy)	Measured/Predicted Dose
PTV Sup Post	674	686	0.98
PTV Inf Post	701	688	1.02
PTV Sup Ant	683	688	0.99
PTV Inf Ant	683	690	0.99
Cord Superior	313	318	0.98
Cord Inferior	309	300	1.03
Parotid Superior	304	308	0.99
Parotid Inferior	321	333	0.96

Table 7-7: TLD Results for Trial 1 from IMRT Plan

TLD Location	Measured Dose (cGy)	Predicted Dose (cGy)	Measured/Predicted Dose
PTV Sup Post	665	686	0.97
PTV Inf Post	679	688	0.99
PTV Sup Ant	675	688	0.98
PTV Inf Ant	681	690	0.99
Cord Superior	314	318	0.99
Cord Inferior	295	300	0.98
Parotid Superior	306	308	0.99
Parotid Inferior	338	333	1.02

Table 7-8: TLD Results for Trial 2 from IMRT Plan



<b>TLD Location</b>	<b>Measured Dose (cGy)</b>	<b>Predicted Dose (cGy)</b>	<b>Measured/Predicted Dose</b>
PTV Sup Post	665	686	0.97
PTV Inf Post	685	688	1.00
PTV Sup Ant	688	688	1.00
PTV Inf Ant	693	690	1.01
Cord Superior	317	318	1.00
Cord Inferior	297	300	0.99
Parotid Superior	297	308	0.97
Parotid Inferior	324	333	0.97

**Table 7-9: TLD Results for Trial 3 from IMRT Plan**

		<b>Film</b>	<b>PRESAGE® Slice</b>	<b>PRESAGE® 3D</b>
<b>Axial Total</b>	3%/3mm	87%	86%	X
	5%/3mm	95%	96%	X
	7%/4mm	99%	99%	X
<b>Sagittal Total</b>	3%/3mm	87%	91%	X
	5%/3mm	94%	98%	X
	7%/4mm	100%	100%	X
<b>Coronal Total</b>	3%/3mm	X	92%	X
	5%/3mm	X	99%	X
	7%/4mm	X	100%	X
<b>Total Volume</b>	3%/3mm	X	X	92%
	5%/3mm	X	X	98%
	7%/4mm	X	X	100%
<b>PTV Total</b>	3%/3mm	X	X	95%
	5%/3mm	X	X	100%
	7%/4mm	X	X	100%
<b>Parotid Total</b>	3%/3mm	X	X	90%
	5%/3mm	X	X	100%
	7%/4mm	X	X	100%
<b>Cord Total</b>	3%/3mm	X	X	83%
	5%/3mm	X	X	99%
	7%/4mm	X	X	100%
<b>Normal Tissue Total</b>	3%/3mm	X	X	93%
	5%/3mm	X	X	97%
	7%/4mm	X	X	100%

**Table 7-10: Percentage of passing pixels for various Gamma Index Restraints for Trial 1 from IMRT Plan**

		<b>Film</b>	<b>PRESAGE® Slice</b>	<b>PRESAGE® 3D</b>
<b>Axial Total</b>	3%/3mm	83%	81%	X
	5%/3mm	92%	92%	X
	7%/4mm	98%	97%	X
<b>Sagittal Total</b>	3%/3mm	84%	91%	X
	5%/3mm	88%	96%	X
	7%/4mm	99%	100%	X
<b>Coronal Total</b>	3%/3mm	X	97%	X
	5%/3mm	X	97%	X
	7%/4mm	X	99%	X
<b>Total Volume</b>	3%/3mm	X	X	88%
	5%/3mm	X	X	94%
	7%/4mm	X	X	99%
<b>PTV Total</b>	3%/3mm	X	X	96%
	5%/3mm	X	X	100%
	7%/4mm	X	X	100%
<b>Parotid Total</b>	3%/3mm	X	X	94%
	5%/3mm	X	X	96%
	7%/4mm	X	X	100%
<b>Cord Total</b>	3%/3mm	X	X	93%
	5%/3mm	X	X	95%
	7%/4mm	X	X	100%
<b>Normal Tissue Total</b>	3%/3mm	X	X	89%
	5%/3mm	X	X	95%
	7%/4mm	X	X	99%

**Table 7-11: Percentage of passing pixels for various Gamma Index Restraints for Trial 2 from IMRT Plan**

		<b>Film</b>	<b>PRESAGE® Slice</b>	<b>PRESAGE® 3D</b>
<b>Axial Total</b>	3%/3mm	85%	88%	X
	5%/3mm	92%	98%	X
	7%/4mm	99%	98%	X
<b>Sagittal Total</b>	3%/3mm	84%	86%	X
	5%/3mm	89%	93%	X
	7%/4mm	98%	100%	X
<b>Coronal Total</b>	3%/3mm	X	94%	X
	5%/3mm	X	99%	X
	7%/4mm	X	98%	X
<b>Total Volume</b>	3%/3mm	X	X	89%
	5%/3mm	X	X	97%
	7%/4mm	X	X	100%
<b>PTV Total</b>	3%/3mm	X	X	97%
	5%/3mm	X	X	100%
	7%/4mm	X	X	100%
<b>Parotid Total</b>	3%/3mm	X	X	100%
	5%/3mm	X	X	100%
	7%/4mm	X	X	100%
<b>Cord Total</b>	3%/3mm	X	X	99%
	5%/3mm	X	X	100%
	7%/4mm	X	X	100%
<b>Normal Tissue Total</b>	3%/3mm	X	X	88%
	5%/3mm	X	X	96%
	7%/4mm	X	X	100%

**Table 7-12: Percentage of passing pixels for various Gamma Index Restraints for Trial 3 from IMRT Plan**

The following code was written to complete analysis in MATLAB. The first section of code exports the dose-line profile from the CERR GUI to Excel for further evaluation.

```
function doseProfileExport(command)
%GC: xlswrite failed on some occasions and was replaced with
%cell2csv, which exports as .csv instead of .xslm.

%RLG 02/2012
%This is a callback file for an Export button in the CERR file
%doseProfileFigure. The mfile can be found in the PlanAnalysis Folder.
%Once a single treatment plan and a single Presage dose is clicked in the
%viewer, press the export button to save to Excel. This is based on
%plotpresage.m

global planC
global stateS
indexS = planC{end}(36);

initialDoseV = [];
initialScanV = [];

hFig=findobj('tag','CERR_DoseLineProfile');
ud=get(hFig,'userdata');
udS=get(ud.slideraxis,'userdata');
xDataL=get(udS.xL,'xData');
x1=xDataL(1);
xDataR=get(udS.xR,'xData');
x2=xDataR(1);

nSamples=stateS.optS.numDoseProfileSamples;
ptsDel=1:nSamples;
ptsL=nSamples/0.95*(x1-0.025);
ptsR=nSamples/0.95*(x2-0.025);
ptsDel=unique([1:floor(ptsL) ceil(ptsR+1e-6):nSamples]);

%get UD stored variables

doseUI=ud.doseUI;
scanUI=ud.scanUI;
nDoses=ud.nDoses;
nScans=ud.nScans;
startPt=ud.startPt;
endPt=ud.endPt;

drawDoses=[];
for i=1:nDoses
    drawDoses(i)=get(doseUI(i),'value');
end
```

```

drawScans=[];
for i=1:nScans
    drawScans(i)=get(scanUI(i),'value');
end

drawDoses=find(drawDoses);
drawScans=find(drawScans);

%Get xyz coord. of samples and distance from first pt

xV=linspace(startPt(1),endPt(1),nSamples);
yV=linspace(startPt(2),endPt(2),nSamples);
zV=linspace(startPt(3),endPt(3),nSamples);
distV=sqrt(sepsq(startPt', [xV;yV;zV]));

for i=1:length(drawDoses)
    doseNum=drawDoses(i);
    transM=getTransM('dose',doseNum,planC);
    if ~isempty(transM)
        [xV1,yV1,zV1]=applyTransM(inv(transM),xV,yV,zV);
    else
        xV1=xV; yV1=yV; zV1=zV;
    end
    dV{i}=getDoseAt(doseNum,xV1,yV1,zV1,planC);
    dV{i}(ptsDel)=NaN;
end

[fileName, pathName]=uiputfile('*.csv','Export Profile');
% GC: extension changed to .csv instead of .xlsm

%outString{1}='Distance';
%outData=outString;
%Edit next line is want to export more than one presage profile. Contibue
%to add dV{i} until complete. Also edit outData
allData=num2cell([distV; dV{1}; dV{2}]);
outData = {'Distance', 'Plan', 'Presage'};
%outData = {'Distance', 'Divided', 'Post', 'Pre'};
plotOutput=cat(1,outData,allData);

cell2csv(fullfile(pathName,fileName),plotOutput);
% GC: xlswrite replaced with cell2csv

end

```

The second piece of code allows for the 2D gamma to be cropped from the full plane to only the area of interest. After CERR calculates the plane of data, the user then can reduce the area of interest to within the dosimeter.

```
function cropGamma
```

```

% crops 2D gamma provided by CERR to size of the dosimeter. A mask is
% created outside of the dosimeter area and set to equal unity and therefore
% not counted in the pass/fail criteria. This is a call back in the
% CERRGammafnc.m that is found in PlanAnalysis\gamma in the CERR folders
% RLG 06/2012

```

```

global stateS
gamma = stateS.gamma.gamma2D;
figure('numbertitle','off','name','Select Dosimeter Area'); imagesc(gamma);
h=impoly;
BW = createMask(h);
mask = gamma;
mask(~BW)=1;
pass = length(find(mask<1));
fail = length(find(mask>1));
total = pass + fail;
xx=[pass fail];
passPer = Roundoff((pass/total)*100,2);
failPer = Roundoff((fail/total)*100,2);
Fig = figure('Name','Cropped Gamma','NumberTitle','off','position',[10 , 10 , 1000 , 600],...
    'resize','off','tag','gamma2dfig');

Axis = axes('parent',Fig,'units', 'pixels','position',[10 ,10 , 580 , 580],'color', [0 0 0], 'XTickLabel', [],...
    'yTickLabel', [], 'xTick', [], 'yTick', []);

clrBarAxis = axes('parent',Fig,'units', 'pixels','position',[595 ,10 , 15 , 550],'color', [0 0 0], 'XTickLabel',
[],...
    'yTickLabel', [], 'xTick', [], 'yTick', []);

imagesc(mask,'parent',Axis), colorbar(clrBarAxis,'peer',Axis);
set(Axis,'XTickLabel', [], 'yTickLabel', [], 'xTick', [], 'yTick', []);

pieAxis = axes('parent',Fig,'units', 'pixels','position',[760 ,350 , 180 , 180],'color', [0 0 0], 'XTickLabel',
[],...
    'yTickLabel', [], 'xTick', [], 'yTick', []);
pie(xx,[0 1],{'Pass=' num2str(passPer) '%'},{'Fail=' num2str(failPer) '%'});
uicontrol(Fig,'Style','text','position',[700, 160, 200, 20],'String',...
    ['DTA = ' num2str(stateS.gamma.DTA *10) ' mm'],'fontsize',10)

uicontrol(Fig,'Style','text','position',[700, 130, 200, 20],'String',...
    ['Dose Diff = ' num2str(stateS.gamma.doseDiff) '%'],'fontsize',10)

uicontrol(Fig,'Style','text','position',[700, 100, 200, 20],'String',...
    ['Max Base Dose = ' num2str(stateS.gamma.refDoseScale) ' GY'],'fontsize',10)

uicontrol(Fig,'Style','text','position',[700, 70, 200, 20],'String',...
    ['Pass = ' num2str(passPer) '% ' ' Fail = ' num2str(failPer) '%'],'fontsize',10)

uicontrol(Fig,'Style','text','position',[700, 30, 200, 20],'String','Pass < 1 Fail > 1','fontsize',10)

uicontrol(Fig,'Style','text','position',[780, 5, 150, 10],'String','Gamma above 2 is snapped to
2','fontsize',7,...
    'fontweight','bold','ForegroundColor',[1 0 0])

```

end



## References

1. Schreiner LJ. Where does gel dosimetry fit in the clinic? *J Phys: Conf Ser.* 2009;164.
2. Low DA, Moran JM, Dempsey JF, Dong L, Oldham M. Dosimetry tools and techniques for IMRT. *Med Phys.* 2011;38(3):1313-38. Epub 2011/04/28. PubMed PMID: 21520843.
3. Low DA, Dempsey JF. Evaluation of the gamma dose distribution comparison method. *Med Phys.* 2003;30(9):2455-64. Epub 2003/10/08. PubMed PMID: 14528967.
4. Kruse JJ. On the insensitivity of single field planar dosimetry to IMRT inaccuracies. *Med Phys.* 2010;37(6):2516-24. Epub 2010/07/17. PubMed PMID: 20632563.
5. Nelms BE, Zhen H, Tome WA. Per-beam, planar IMRT QA passing rates do not predict clinically relevant patient dose errors. *Med Phys.* 2011;38(2):1037-44. Epub 2011/04/02. PubMed PMID: 21452741; PubMed Central PMCID: PMC3188652.
6. Ibbott GS, Followill DS, Molineu HA, Lowenstein JR, Alvarez PE, Roll JE. Challenges in credentialing institutions and participants in advanced technology multi-institutional clinical trials. *Int J Radiat Oncol Biol Phys.* 2008;71(1 Suppl):S71-5. Epub 2008/05/24. doi: S0360-3016(07)04287-3 [pii]

7. Clift C, Thomas A, Adamovics J, Chang Z, Das I, Oldham M. Toward acquiring comprehensive radiosurgery field commissioning data using the PRESAGE/optical-CT 3D dosimetry system. *Phys Med Biol.* 2010;55(5):1279-93. Epub 2010/02/06. doi: S0031-9155(10)34385-5 [pii]
8. Oldham M, Guo P, Gluckman G, Adamovics J. IMRT verification using a radiochromic/optical-CT dosimetry system. *J Phys.* 2006;56:221-4. Epub 2007/04/27. doi: 10.1088/1742-6596/56/1/033. PubMed PMID: 17460782; PubMed Central PMCID: PMC1855091.
9. Gum F, Scherer J, Bogner L, Solleder M, Rhein B, Bock M. Preliminary study on the use of an inhomogeneous anthropomorphic Fricke gel phantom and 3D magnetic resonance dosimetry for verification of IMRT treatment plans. *Phys Med Biol.* 2002;47(7):N67-77. Epub 2002/05/09. PubMed PMID: 11996066.
10. Day MJ, Stein G. Chemical effects of ionizing radiation in some gels. *Nature.* 1950;166(4212):146-7. Epub 1950/07/22. PubMed PMID: 15439181.
11. Gore JC, Kang YS, Schulz RJ. Measurement of radiation dose distributions by nuclear magnetic resonance (NMR) imaging. *Phys Med Biol.* 1984;29(10):1189-97. Epub 1984/10/01. PubMed PMID: 6494247.
12. De Deene Y, Venning A, Hurley C, Healy BJ, Baldock C. Dose-response stability and integrity of the dose distribution of various polymer gel dosimeters. *Physics in medicine and biology.* 2002;47(14):2459-70. PubMed PMID: 12171334.

13. De Deene Y, Hurley C, Venning A, Vergote K, Mather M, Healy BJ, Baldock C. A basic study of some normoxic polymer gel dosimeters. *Physics in medicine and biology*. 2002;47(19):3441-63. PubMed PMID: 12408474.
14. Fong PM, Keil DC, Does MD, Gore JC. Polymer gels for magnetic resonance imaging of radiation dose distributions at normal room atmosphere. *Phys Med Biol*. 2001;46(12):3105-13. PubMed PMID: 11768494.
15. Adamovics J, Maryanski M. New 3D radiochromic solid polymer dosimeter from leuco dyes and a transparent polymeric matrix. *Med Phys*. 2003;30:1349.
16. Adamovics J, Maryanski MJ. Characterisation of PRESAGE: A new 3-D radiochromic solid polymer dosemeter for ionising radiation. *Radiat Prot Dosimetry*. 2006;120(1-4):107-12. Epub 2006/06/20. doi: nci555 [pii]
17. Pedersen TV, Olsen DR, Skretting A. Measurement of the ferric diffusion coefficient in agarose and gelatine gels by utilization of the evolution of a radiation induced edge as reflected in relaxation rate images. *Physics in medicine and biology*. 1997;42(8):1575-85. PubMed PMID: 9279907.
18. Guo PY, Adamovics JA, Oldham M. Characterization of a new radiochromic three-dimensional dosimeter. *Med Phys*. 2006;33(5):1338-45. Epub 2006/06/07. PubMed PMID: 16752569; PubMed Central PMCID: PMC1616190.

19. Oldham M, Guo P, Gluckman G, Adamovics J. IMRT verification using a radiochromic/optical-CT dosimetry system. *Journal of physics Conference series*. 2006;56:221-4. doi: 10.1088/1742-6596/56/1/033. PubMed PMID: 17460782; PubMed Central PMCID: PMC1855091.
20. Skyt PS, Balling P, Petersen JB, Yates ES, Muren LP. Temperature dependence of the dose response for a solid-state radiochromic dosimeter during irradiation and storage. *Medical physics*. 2011;38(5):2806-11. PubMed PMID: 21776817.
21. Bushberg JT. *The essential physics of medical imaging*. Philadelphia: Lippincott Williams & Wilkins; 2002.
22. Newton J, Thomas A, Ibbott G, Oldham M. Preliminary commissioning investigations with the DMOS-RPC optical-CT Scanner. *Journal of physics Conference series*. 2010;250(1):12078. doi: 10.1088/1742-6596/250/1/012078. PubMed PMID: 21218171; PubMed Central PMCID: PMC3015184.
23. Knoll GF. *Radiation detection and measurement / Glenn F. Knoll*. 3rd ed. New York: John Wiley & Sons; 2000. xiv, 802 p. p.
24. Richley L, John AC, Coomber H, Fletcher S. Evaluation and optimization of the new EBT2 radiochromic film dosimetry system for patient dose verification in radiotherapy. *Physics in medicine and biology*. 2010;55(9):2601-17. doi: 10.1088/0031-9155/55/9/012. PubMed PMID: 20393235.

25. Harms WB, Sr., Low DA, Wong JW, Purdy JA. A software tool for the quantitative evaluation of 3D dose calculation algorithms. *Medical physics*. 1998;25(10):1830-6. PubMed PMID: 9800688.
26. Low DA, Harms WB, Mutic S, Purdy JA. A technique for the quantitative evaluation of dose distributions. *Medical physics*. 1998;25(5):656-61. PubMed PMID: 9608475.
27. Pulliam KB, Huang JY, Howell RM, Followill D, Bosca R, O'Daniel J, Kry SF. Comparison of 2D and 3D gamma analyses. *Med Phys*. 2014;41(2):021710. doi: 10.1118/1.4860195. PubMed PMID: 24506601; PubMed Central PMCID: PMC3977814.
28. Oldham M, Thomas A, O'Daniel J, Juang T, Ibbott G, Adamovics J, Kirkpatrick JP. A Quality Assurance Method that Utilizes 3D Dosimetry and Facilitates Clinical Interpretation. *Int J Radiat Oncol Biol Phys*. 2012. Epub 2012/03/01. doi: S0360-3016(11)03670-4 [pii]
29. Bentzen SM, Constine LS, Deasy JO, Eisbruch A, Jackson A, Marks LB, Ten Haken RK, Yorke ED. Quantitative Analyses of Normal Tissue Effects in the Clinic (QUANTEC): an introduction to the scientific issues. *Int J Radiat Oncol Biol Phys*. 2010;76(3 Suppl):S3-9. Epub 2010/03/05. doi: S0360-3016(09)03300-8 [pii]
30. Lyman JT. Complication probability as assessed from dose-volume histograms. *Radiat Res Suppl*. 1985;8:S13-9. Epub 1985/01/01. PubMed PMID: 3867079.

31. Kutcher GJ, Burman C, Brewster L, Goitein M, Mohan R. Histogram reduction method for calculating complication probabilities for three-dimensional treatment planning evaluations. *Int J Radiat Oncol Biol Phys.* 1991;21(1):137-46. Epub 1991/05/15. doi: 0360-3016(91)90173-2 [pii]. PubMed PMID: 2032884.
32. Technical Basis of Radiation Therapy. Levitt S, Purdy J, Perez C, Poortmans P, editors: Springer Berlin Heidelberg; 2012.
33. Niemierko A. Reporting and analyzing dose distributions: a concept of equivalent uniform dose. *Med Phys.* 1997;24(1):103-10. Epub 1997/01/01. PubMed PMID: 9029544.
34. Deasy JO, Blanco AI, Clark VH. CERR: a computational environment for radiotherapy research. *Med Phys.* 2003;30(5):979-85. Epub 2003/05/30. PubMed PMID: 12773007.
35. Sakhalkar HS, Oldham M. Fast, high-resolution 3D dosimetry utilizing a novel optical-CT scanner incorporating tertiary telecentric collimation. *Med Phys.* 2008;35(1):101-11. Epub 2008/02/26. PubMed PMID: 18293567; PubMed Central PMCID: PMC2504744.
36. Sakhalkar HS, Adamovics J, Ibbott G, Oldham M. A comprehensive evaluation of the PRESAGE/optical-CT 3D dosimetry system. *Med Phys.* 2009;36(1):71-82. Epub 2009/02/25. PubMed PMID: 19235375; PubMed Central PMCID: PMC2673667.
37. Newton J, Thomas A, Ibbott GS, Oldham M. Preliminary commissioning investigations with the DMOS-RPC optical-CT Scanner. *J Phys: Conf Ser.* 2010;250. doi: 10.1088/1742-6596/250/1/012078.

38. Followill DS, Evans DR, Cherry C, Molineu A, Fisher G, Hanson WF, Ibbott GS. Design, development, and implementation of the radiological physics center's pelvis and thorax anthropomorphic quality assurance phantoms. *Med Phys.* 2007;34(6):2070-6. Epub 2007/07/28. PubMed PMID: 17654910.
39. Juang T, Grant R, Adamovics J, Ibbott G, Oldham M. On the feasibility of comprehensive high-resolution 3D remote dosimetry. *Medical physics.* 2014;41(7):071706. doi: 10.1118/1.4884018. PubMed PMID: 24989375; PubMed Central PMCID: PMC4105963.
40. Gorjiara T, Hill R, Kuncic Z, Adamovics J, Bosi S, Kim JH, Baldock C. Investigation of radiological properties and water equivalency of PRESAGE dosimeters. *Medical physics.* 2011;38(4):2265-74. PubMed PMID: 21626961.
41. Skyt PS, Balling P, Petersen JBB, Yates ES, Muren LP. Temperature dependence of the dose response for a solid-state radiochromic dosimeter during irradiation and storage. *Medical Physics.* 2011;38(5):2806-11. doi: Doi 10.1118/1.3582702. PubMed PMID: ISI:000290625700056.
42. Vidovic AK, Juang T, Meltsner S, Adamovics J, Chino J, Steffey B, Craciunescu O, Oldham M. An investigation of a PRESAGE(R) in vivo dosimeter for brachytherapy. *Physics in medicine and biology.* 2014;59(14):3893-905. doi: 10.1088/0031-9155/59/14/3893. PubMed PMID: 24957850; PubMed Central PMCID: PMC4136760.
43. Thomas A, Newton J, Adamovics J, Oldham M. Commissioning and benchmarking a 3D dosimetry system for clinical use. *Med Phys.* 2011.

44. Skyt PS, Balling P, Petersen JB, Yates ES, Muren LP. Effect of irradiation and storage temperature on PRESAGE dose response. *J Phys: Conf Ser.* 2010;250.
45. Jackson J, Juang T, Adamovics J, Oldham M. An investigation of PRESAGE(R) 3D dosimetry for IMRT and VMAT radiation therapy treatment verification. *Physics in medicine and biology.* 2015;60(6):2217-30. doi: 10.1088/0031-9155/60/6/2217. PubMed PMID: 25683902.
46. Mostaar A, Hashemi B, Zahmatkesh MH, Aghamiri SM, Mahdavi SR. A basic dosimetric study of PRESAGE: the effect of different amounts of fabricating components on the sensitivity and stability of the dosimeter. *Phys Med Biol.* 2010;55(3):903-12. Epub 2010/01/15. doi: S0031-9155(10)28599-8 [pii]  
10.1088/0031-9155/55/3/023. PubMed PMID: 20071770.
47. Molineu A, Followill DS, Balter PA, Hanson WF, Gillin MT, Huq MS, Eisbruch A, Ibbott GS. Design and implementation of an anthropomorphic quality assurance phantom for intensity-modulated radiation therapy for the Radiation Therapy Oncology Group. *International journal of radiation oncology, biology, physics.* 2005;63(2):577-83. doi: 10.1016/j.ijrobp.2005.05.021. PubMed PMID: 16168849.
48. Dijkema T, Raaijmakers CP, Ten Haken RK, Roesink JM, Braam PM, Houweling AC, Moerland MA, Eisbruch A, Terhaard CH. Parotid gland function after radiotherapy: the combined michigan and utrecht experience. *Int J Radiat Oncol Biol Phys.* 2010;78(2):449-53. doi: 10.1016/j.ijrobp.2009.07.1708. PubMed PMID: 20056347; PubMed Central PMCID: PMC2889151.



49. Ezzell GA, Burmeister JW, Dogan N, LoSasso TJ, Mechalakos JG, Mihailidis D, Molineu A, Palta JR, Ramsey CR, Salter BJ, Shi J, Xia P, Yue NJ, Xiao Y. IMRT commissioning: multiple institution planning and dosimetry comparisons, a report from AAPM Task Group 119. *Medical physics*. 2009;36(11):5359-73. PubMed PMID: 19994544.
50. Chung H, Jin H, Palta J, Suh TS, Kim S. Dose variations with varying calculation grid size in head and neck IMRT. *Phys Med Biol*. 2006;51(19):4841-56. Epub 2006/09/21. doi: S0031-9155(06)20506-2 [pii]  
10.1088/0031-9155/51/19/008. PubMed PMID: 16985274.
51. Yan G, Liu C, Simon TA, Peng LC, Fox C, Li JG. On the sensitivity of patient-specific IMRT QA to MLC positioning errors. *Journal of applied clinical medical physics / American College of Medical Physics*. 2009;10(1):2915. PubMed PMID: 19223841.
52. Niemierko A, Goitein M. The influence of the size of the grid used for dose calculation on the accuracy of dose estimation. *Medical physics*. 1989;16(2):239-47. PubMed PMID: 2541326.

## VITA

Ryan Grant Lafratta was born in St. Petersburg, Florida on April 3, 1985, the daughter Caren Cardwell Grant and Walter Henry Grant III. After completing her work at Bellaire Senior High School, Bellaire, Texas in 2003, she entered The University of Texas at Austin in Austin, Texas. She received the degree of Bachelor of Science with a major in physics from Texas in May, 2007. In August of 2007 she entered The University of Texas Graduate School of Biomedical Sciences at Houston. She received the degree of Master of Science with a major in Medical Physics in May, 2010.

Permanent Address:

5317 Pocahontas St

Bellaire, TX 77401